Distinct Responses To Reduplicated Chromosomes Require Distinct Mad2 Responses

Benjamin M. Stormo[1] and Donald T. Fox[1,2]

1) Department of Cell Biology

2) Department of Pharmacology & Cancer Biology

Duke University Medical Center

DUMC Box 3813

Durham, NC 27710

e-mail for correspondence: don.fox@duke.edu

ABSTRACT

Duplicating chromosomes once each cell cycle produces sister chromatid pairs, which separate accurately at anaphase. In contrast, reduplicating chromosomes without separation frequently produces polytene chromosomes, a barrier to accurate mitosis. Chromosome reduplication occurs in many contexts, including: polytene tissue development, polytene tumors, and following treatment with mitosis-blocking chemotherapeutics. However, mechanisms responding to or resolving polyteny during mitosis are poorly understood. Here, using *Drosophila,* we uncover two distinct reduplicated chromosome responses. First, when reduplicated polytene chromosomes persist into metaphase, an anaphase delay prevents tissue malformation and apoptosis. Second, reduplicated polytene chromosomes can also separate prior to metaphase through a spindle-independent mechanism termed Separation-Into-Recent-Sisters (SIRS). Both reduplication responses require the spindle assembly checkpoint protein Mad2. While Mad2 delays anaphase separation of metaphase polytene chromosomes, Mad2's control of overall mitotic timing ensures efficient SIRS. Our results pinpoint mechanisms enabling continued proliferation after genome reduplication, a finding with implications for cancer progression and prevention.

INTRODUCTION

Regulating mitotic chromosome structure is critical to preventing genomic instability (Gordon *et al.*, 2012; Pfau & Amon, 2012). During mitosis, chromatids associate in sister pairs, which facilitates their bi-orientation and subsequent segregation to opposite spindle poles. A frequently occurring and long-recognized departure from this paired chromosome structure occurs when the genome reduplicates without chromatid separation (hereafter: genome reduplication). Following a single extra S-phase, cells frequently form diplochromosomes: four sister chromatids conjoined at centromeres (White, 1935). A more general term for chromosomes formed by any degree of genome reduplication without chromatid separation is "polytene" (Painter, 1934; Zhimulev *et al.*, 2004). Mitosis in polytene cells is considered "ill-advised for mechanical reasons" (Edgar & Orr-Weaver, 2001). Indeed, separation of polytene diplochromosomes at anaphase causes chromosome mis-segregation (Vidwans *et al.*, 2002).

Given this association of polytene chromosomes with mitotic errors, it is not surprising that these structures are often associated with aberrant development and disease. Polytene chromosomes have been observed in cells from spontaneous human abortions (Therman *et al.*, 1978), in muscular dystrophy patients (Schmidt *et al.*, 2011), in a variety of tumors (Biesele & Poyner, 1943; Erenpreisa *et al.*, 2009; Levan & Hauschka, 1953; Therman *et al.*, 1983) and can also precede tumor formation in mice (Davoli & de Lange, 2012). Polytene chromosomes also occur after treatment with currently used anti-mitotic chemotherapeutics such as those that inhibit Topoisomerase II (Cantero *et al.*, 2006; Sumner, 1998). Disruption of numerous other processes crucial for mitosis, including spindle formation (Goyanes & Schvartzman, 1981; Takanari *et al.*, 1985) sister chromatid cohesion (Wirth *et al.*, 2006) or genome integrity control (Davoli *et al.*, 2010) also cause genome reduplication and polyteny. Thus, polytene

chromosomes, a source of mitotic instability, are a conserved and common outcome of ectopic genome reduplication.

To understand how cells adapt the cell cycle machinery to the challenge of segregating polytene chromosomes, naturally occurring models of this problem can prove useful. Programmed genome reduplication cycles of successive S-phase without M-phase (endocycles, Edgar *et al.*, 2014; Fox & Duronio, 2013 see nomenclature) produce polytene chromosomes in many plant, insect, and mammalian species, including humans (Zhimulev *et al.*, 2004; Zybina & Zybina, 1996). However, many cells with programmed genome reduplication do not subsequently divide, preventing study of how nature has circumvented the issue of segregating polytene chromosomes. In contrast, we previously demonstrated that rectal papilla (hereafter: papillar cells), ion-absorbing structures in the *Drosophila* hindgut, are built entirely by mitosis of endocycled cells (Fox *et al.*, 2010; Schoenfelder *et al.*, 2014). Surprisingly, we never observed polytene chromosomes in hundreds of papillar metaphases (Fox *et al.*, 2010; Schoenfelder *et al.*, 2014), suggesting papillar cells are programmed to either avoid or eliminate polyteny and its associated mitotic defects. Interestingly, previous studies suggest that polyteny can be at least partially undone without anaphase in both normal and tumorous tissue (Dej & Spradling, 1999; Grell, 1946; Levan & Hauschka, 1953). Thus, in some cases of genome reduplication, polyteny may be actively regulated or eliminated.

Taken together, the potential negative impact of genome reduplication on mitotic chromosome structure is clear. However, the responses that enable either developing or tumorous cells to continue dividing after reduplication, despite profound chromosome structure changes, remain unclear. Here, using *Drosophila* tissue models of both ectopic and naturally occurring genome reduplication, we uncover two distinct

cellular responses to reduplicated chromosomes. Both reduplication responses require the conserved spindle assembly checkpoint (SAC) protein Mad2, which inhibits the Anaphase Promoting Complex to both delay anaphase in response to unattached or tensionless kinetochores and to also regulate overall mitotic timing from nuclear envelope breakdown (NEBD) to anaphase onset (London & Biggins, 2014; Musacchio, 2015). In reduplicated cells that retain polytene chromosomes at metaphase, we show Mad2 is involved in a SAC wait-anaphase response. This anaphase delay does not fully prevent the mitotic errors and the resulting aneuploidy associated with mitosis of polytene chromosomes, but it substantially prevents apoptosis, tissue malformation, and organismal death. In contrast to this SAC response, we also define a second response in reduplicated cells that actively eliminates polyteny before anaphase. In this response, polytene chromosomes undergo a dynamic, spindle-independent process we term Separation Into Recent Sister chromatid pairs (SIRS), which eliminates any trace of polyteny before anaphase. Unlike mitosis with metaphase polytene chromosomes, mitosis with SIRS does not trigger a Mad2-dependent anaphase delay. Yet, we find Mad2 promotes efficient SIRS by allowing sufficient time between nuclear envelope breakdown and anaphase, which allows polytene chromosomes to separate into conventional mitotic sister chromatid pairs. Our results therefore define two distinct responses to reduplicated chromosomes, each of which depends on a distinct Mad2 response.

RESULTS

To understand the mechanisms employed by cells with reduplicated chromosomes, we took advantage of accessible developmental models and *in vivo* genetic tools in *Drosophila*. While ectopic genome reduplication was previously established to generate polytene diplochromosomes and subsequent mitotic errors in *Drosophila*, the effects were examined within the time-frame of the terminal embryonic mitotic cell cycle (Vidwans *et al.*, 2002). Thus, the long-term effects of ectopic genome reduplication on cell

viability and tissue development, and key molecular regulation of reduplicated chromosomes has remained unexplored. In parallel, our development of rectal papillae as a non-ectopic, naturally occurring model of mitosis after genome reduplication enabled us to also study how cells programmed to undergo genome reduplication can regulate polytene chromosome structure during mitosis.

Ectopic genome reduplication yields polyteny and continued aneuploid cell division

We first ectopically induced genome reduplication in proliferating tissues of developing larvae by transiently re-programming mitotic cycles to endocycles. *fizzy-related* (*fzr,* mammalian *Cdh1*) plays a conserved role in endocycles by targeting the anaphase promoting complex to destroy the mitotic Cyclins A, B, and B3 (Larson-Rabin *et al.*, 2008; Sigrist & Lehner, 1997). *fzr* overexpression was previously shown to transform mitotic cycles into endocycles (Sigrist & Lehner, 1997). To transiently induce endocycles, we used a brief heat shock (HS) pulse to express ectopic *fzr* (*HS>fzr*, **Fig1A**). Using the cell cycle marker system Fly-FUCCI (Zielke *et al.*, 2014 **Fig1B**) we find that pulsed *fzr* overexpression temporarily eliminates expression of the S/G2/M mRFP-CyclinB reporter in wing imaginal disc cells (**Fig1C vs. C',D**)**.** This same population of mRFP-CyclinB-negative cells continues to express the G2/M/G1 GFP-E2F1 reporter, but in greater proportion (**Fig1C vs. C', D**). Together, these data suggest *HS>fzr* promotes G1 accumulation (91% of cells compared to 36% in controls, **Fig1B-D**). To test whether this G1 accumulation is due to direct conversion of G2 cells to G1, as opposed to an acceleration of the cell cycle through G2/M, we stained for the mitotic marker Phospho-Histone H3 at several time points after pulsed *fzr* expression. For up to 7 hours after *fzr* overexpression, there is essentially no mitosis in the wing imaginal disc, whereas wing cells in heat shocked wild type flies continue to divide after heat shock (**FigS1A,B**). Based on previous studies of *fzr* function and our FUCCI and Phospho-Histone H3 data, we conclude that pulsed *fzr* expression converts G2 cells to a G1 state by eliminating mitotic cyclins (**Fig1A**).

To determine if the G2 cells re-programmed to G1 proceed through a second genome duplication, we examined mitotic chromosome number when mitosis of *HS>fzr* tissue first resumes (ten hours after heat shock). At this time-point, we observe frequent tetraploidy (41% of mitotic cells, equivalent to 93% of all G2 cells prior to heat shock, **Fig1F,F',H**). We obtained similar results when examining the results of *fzr* overexpression in diploid brain progenitors (**FigS1C**)**.** These results confirm our ability to induce genome reduplication in normally diploid tissues. We also examined chromosome structure in our induced tetraploid cells. When *HS>fzr*-induced tetraploid DNA first condenses post-heat shock, all chromatids of each chromosome type are closely aligned in a polytene configuration, as evidenced by having the haploid number of distinguishable chromosomes (four in females, **Fig1F**). Frequently, we observe un-pairing of the homologous groups of centromeres within each polytene chromosome (**Fig1F**, asterisk, also see discussion). Later, at the first metaphase, homologous chromosomes of each polytene are now completely separated, but the four centromeres of each group of sister chromatids remain conjoined within diplochromosomes (observed for 96% of tetraploid cells, **Fig1F' inset, H**). Thus, *HS>fzr* induces ectopic genome reduplication, resulting in tetraploid cells with metaphase polytene diplochromosomes.

We next examined the mitotic fidelity of cells with diplochromosomes by two independent means: chromosome karyotype analysis and live imaging. By examining the metaphase chromosomes of the division immediately following diplochromosome division, we could detect whether aneuploidy results from diplochromosome segregation. Following the division of cells with diplochromosomes, we observe tetraploid-aneuploid cells with one or two extra or missing chromosomes (8.6% of mitotic cells). In these cells, diplochromosomes are no longer present and instead chromatids are found in distinct sister pairs (**Fig1G**). This suggests that during or after anaphase of the first post-reduplication division,

145 diplochromosomes can separate into individual chromatids. Further, these diplochromosome divisions
146 can produce aneuploid daughter cells, many of which continue to divide (**Fig1G,H,K, FigS1D**).

147

148 We also live imaged mitosis of wing imaginal disc and brain progenitor (neuroblasts and ganglion mother)
149 cells, both with and without ectopic genome reduplication. In addition to using a histone marker to
150 observe chromosomes, we used the Cenp-C-Tomato marker to observe kinetochores. Control diploid cells
151 divide without errors (**Fig1I,J No HS, Movie S1A**). In contrast, most (85%) tetraploid divisions with
152 diplochromosomes exhibit lagging chromosomes (**Fig1I,J, HS+10hr, Movie S1B**). In some of these divisions
153 we clearly observe four chromatids of a diplochromosome segregating 3:1 (in agreement with prior work
154 in embryos by Vidwans *et al., 2002)*, suggesting incomplete or imprecise sister chromatid disjunction is
155 the cause of chromosome gains and losses (**Fig 1I, FigS1D, Movie S1B**). These errors appear to result
156 primarily from diplochromosomes and not tetraploidy itself, as tetraploid cells in the subsequent divisions
157 (which lack diplochromosomes) have a substantially reduced error rate (**Fig1J, S1E, MovieS1C).** In spite of
158 the high initial error rate caused by separation of diplochromosomes, tetraploid-aneuploid cell divisions
159 continue to occur for at least 5 days after genome reduplication, as determined by cytology (**Fig1H**
160 **HS+120hr**). We conclude that division of diplochromosomes in the mitotically expanding diploid
161 progenitor tissues that we surveyed can lead to the generation of aneuploid cells, which can continue to
162 divide (**Fig1K).**

163

164 To determine the long-term effect of tetraploid-aneuploid divisions on tissue development, we took
165 advantage of the fact that expression of *HS>fzr* occurs in adult progenitor tissues. We thus examined the
166 survival of these animals to adulthood. Survival is only subtly affected in animals with mild (23.0%

tetraploid [S.E.M. 4.9%]) levels of induced error-prone tetraploid progenitor division (**Fig2A**), and resulting adult tissues appear normal (**Fig2B**). In contrast, when tetraploidy is further increased by increasing the duration of heat shock, organism survival decreases in a tetraploid-dependent fashion (**Fig2A, FigS2A**). Together, these results show that ectopic genome reduplication yields tetraploid cells with polytene metaphase diplochromosomes, which are aneuploid-prone **(Fig1K).** These conclusions are in agreement with a previous study (Vidwans et al, 2002). We further show that such aneuploid-prone cells can continue to propagate, and that only at high frequencies are these error-prone tetraploid mitotic events lethal to the organism.

Polyteny response 1: Spindle assembly checkpoint (SAC)-mediated anaphase delay

Our data (**Fig1H, FigS1C)** and those of others (Vidwans *et al.*, 2002) suggest that many polytene diplochromosome divisions in a variety of tissues do not lead to aneuploidy. Little is known about aneuploidy prevention mechanisms in cells with polytene chromosomes, despite the numerous mechanisms that can generate these aberrations. Through live imaging, we uncovered one such aneuploidy-prevention mechanism in cells with metaphase diplochromosomes. Because our heat shock protocol only affects cells in G2, a single *HS>fzr* pulse creates a mixed population of unaltered diploid cells and diplochromosome-containing tetraploid cells. Allowing us to simultaneously live image both cell types in the same tissue. Metaphase in cells with diplochromosomes (**Fig2C,** yellow dotted outline) is significantly longer than in diploid cells (**Fig2C** blue dashed outline, **Fig2D**), consistent with previous work (Pandey *et al.*, 2005). We thus hypothesized that diplochromosomes trigger the SAC, which activates a wait-anaphase signal until all kinetochores attach to microtubules and are under tension (London & Biggins, 2014; Musacchio, 2015). To test this model, we examined SAC-defective *mad2* null animals (Buffin *et al.*, 2007; Emre *et al.*, 2011 **FigS2B**). Using live imaging of wing imaginal discs before and after heat

shock, we find that loss of *mad2* eliminates the lengthened period of metaphase caused by diplochromosomes (**Fig2D**). From these data, we conclude that diplochromosomes trigger a SAC wait-anaphase response.

Although important for mitosis in cultured *Drosophila* S2 cells (Orr *et al.*, 2007), the Mad2-directed SAC is reported to be dispensable in *Drosophila* tissue mitosis (Buffin *et al.*, 2007; Emre *et al.*, 2011). *mad2* null animals are viable with no obvious tissue defects (**Fig2B** Buffin *et al.*, 2007) due in part to an apoptotic response (Morais da Silva *et al.*, 2013). In contrast, the Mad2 SAC response is essential during development of *HS>fzr* animals. Even at low levels of tetraploidy, which affect the survival of *HS>fzr* animals only slightly, few *HS>fzr, mad2* animals survive to adulthood (15.4%, **Fig2A, S2A**). To understand why *HS>fzr, mad2* animals have defects, we analyzed the surviving animals. In these animals, we find a variety of developmental defects in normally diploid tissues, including smaller eyes, ectopic wing veins, and melanotic abdominal masses (**Fig2B**). Increased apoptosis is associated with these tissue malformation phenotypes, as progenitor tissue from *HS>fzr, mad2* animals have much higher rates of apoptotic cell death as shown by both TUNEL labeling (**Fig2E,F**), and cleaved caspase staining (**FigS2C,D**). Taken together, our data identify an important role for the Mad2-dependent SAC in delaying anaphase in the presence of metaphase polytene diplochromosomes.

Polyteny response 2: Separation Into Recent Sisters (SIRS)

Having defined a response to mitosis after ectopic genome reduplication, we next asked if this same mechanism operates in a tissue that we previously found to divide after programmed genome reduplication. In earlier work we found *Drosophila* rectal papillar cells (hereafter: papillar cells) naturally

undergo two *fzr*-dependent endocycles during the 2nd larval instar to generate octoploid cells and then divide, on average, two times during pupal development. An intervening S-phase accompanies these polyploid divisions, and cells at the papillar base undergo one additional S-phase after the final polyploid mitosis (**Fig3A** Fox *et al.*, 2010; Schoenfelder *et al.*, 2014). Thus, as with *HS>fzr* induction in diploid tissues, papillar development naturally involves genome reduplication followed by mitosis. Our previous work established that papillar mitoses can be error prone, so the same problems with dissociating polytene chromosomes in *HS>fzr* tissues could be responsible for a portion of these errors during papillar divisions. However, we previously did not see, in hundreds of observed cells, any instances of metaphases with persistent polyteny in papillar cells, suggesting that papillar cells somehow avoid mitosis of polytene chromosomes. If papillar cells were to behave like cells that undergo ectopic genome reduplication, one would expect first division papillar chromosomes to be arranged in quadruplochromosomes, reflecting one additional genome doubling relative to cells with diplochromosomes. Instead, through careful re-examination of the first octoploid metaphase, we confirmed that papillar chromosomes do not have quadruplochromosomes, but instead chromatids in these octoploid cells are arranged in individual sister chromatid pairs (**Fig3B'' inset, C**). This suggested two possibilities: 1) papillar cells never form polytenes, or 2) papillar cells form polytenes, but somehow separate into recent sister pairs prior to the first metaphase.

To distinguish these two possibilities, we examined papillar karyotypes from the moment chromosome condensation could be detected. Papillar cells re-enter mitosis from a G2-like state, as evidenced by expression of the G2/M regulator Cdc25/string just before the onset of pupal cell cycles (Fox *et al.*, 2010) (**Fig S3A**). At time points early in the first mitosis, we indeed find that papillar chromosomes are polytene (**Fig3B, Polytene**). In these polytenes, we again see examples of cells where the centromeric regions are

no longer tightly associated, as we did in our studies of *HS>fzr*-induced polyteny. However, unlike in cells with induced polyteny, the centromeres in papillar polytene cells are able to not only separate into groups of homologs, but to further separate into individual sister chromatid pairs (asterisks in **Fig 3B and FigS3C** vs. **Fig 1F**, also see discussion). At this early mitotic time point, we also observe cells where polytenes are absent. Instead, in these cells, sister chromatid pairs and homologs of each chromosome type are separated but remain clumped closely together, as if the polytene chromosome recently separated into pairs containing only the most recent sister chromatids (**Fig3B', D, Clumped**). Neither the polytene nor the clumped configurations remain during the second division (**Fig3C, D**), suggesting a specific chromosome structure is present early in the first division of papillar cells. Similarly, by Fluorescent *In Situ* Hybridization (FISH) we find examples of both closely associated (polytene) and dispersed (separated/non-polytene) signals during the period of the first papillar mitosis (**FigS3B**). Thus, a key difference between the response to genome reduplication between papillar and *HS>fzr* cells is the elimination of polyteny before anaphase in papillar cells.

To examine if a majority of (if not all) papillar cells transition from polytene to separate/non-polytene chromosomes during the first mitosis, we used drug treatment to isolate specific chromosome structures during the transition into the first papillar division. To enrich for early mitotic and pre-mitotic chromosomes, we induced Premature Chromosome Compaction (PCC) in papillar cells at a time point just prior to the first mitosis (Methods). PCC causes interphase chromosomes to condense and makes it possible to visualize interphase chromosome structure by standard cytological methods **(FigS3C)**. Using this technique we find that in pre-mitotic papillar tissue, clear polytene chromosomes are present in nearly every cell **(Fig 3D Pre 1st Div, FigS3C)**. If we instead enrich for cells in metaphase of the first mitosis by treating with the spindle poison colcemid, we find zero examples where chromosomes are still

polytene. In these metaphase-enriched samples, all chromosomes are separated into recent-sister pairs, and even cells with clumped chromosomes are rare (**Fig3D, 1st Div +colc**). Thus, our pharmacological studies further suggest that essentially all genome-reduplicated papillar cells are programmed to completely eliminate polytene chromosomes as cells progress into the first metaphase.

To observe the temporal dynamics of the pre-anaphase elimination of papillar polyteny, we used live imaging, using the same markers used to image diplochromosome division. Prior to the first papillar mitosis, the kinetochores from each homolog are closely associated into an average of 4.1 large foci, close to the haploid number of distinct chromosomes (4 for females and 5 for males due to X/Y un-pairing, **Fig 3E**). As time progresses in the first division, it is possible to watch these large kinetochore foci disperse into many smaller foci prior to metaphase (**Fig3F, inset**). In contrast, prior to the second division kinetochores are already separated into many more foci (an average of 15.1 observably distinct foci per cell) before entry into mitosis (**Fig3E**). During the second division, the number of resolvable foci remains essentially constant (**Fig3G**). Additionally, the histone marker reveals that polytene chromosomes are visible when chromosomes first condense and can then be seen to disperse during the first but not the second division (**Fig3F v. Fig3G**, **-18:00 min**). This result confirms the model that genome-reduplicated papillar cells eliminate polyteny during the first mitosis, then undergo an intervening S-phase before the next division (**Fig3A**). We also confirmed that each clump of 4 or 5 pre-first division centromeres only contains a single chromosome type. To do so, we took advantage of the fact that dosage compensation in flies relies on upregulation of transcription on the male X chromosome via the Dosage Compensation Complex (DCC, Conrad & Akhtar, 2012). By live imaging papillar cells expressing the DCC complex protein MSL3 tagged with GFP, which localizes only to the male X-chromosome (Strukov *et al.*, 2011), we find that indeed only a single Cenp-C-Tomato focus is MSL3-GFP positive prior to polytene dissociation (**FigS3D,**

Movie S3C). Taken together, we find papillar cells avoid mitosis of polytene chromosomes in part by undergoing a pre-anaphase chromosome separation process we term Separation Into Recent Sisters (SIRS, **Fig3H**).

Previously, we confirmed that a similar polyploid mitotic program occurs in the developing hindgut of the mosquito *Culex pipiens* (Fox *et al.*, 2010). In this tissue, we observe mitotic polytene chromosomes only during the early period of the first polyploid mitosis (**FigS3E, MovieS3D**). This result is consistent with previous classical descriptions of this process that suggested a polytene organization is present only early in the first polyploid mitosis (Grell, 1946). From our *Drosophila* and *Culex* studies, we conclude that unlike cells that enter metaphase with polytene chromosomes, a separate mechanism, SIRS, can eliminate polyteny as cells enter metaphase.

Spindle-independent mitotic timing by Mad2 promotes efficient SIRS

Our dual genome-reduplication systems identified two distinct cellular responses to polytene chromosomes: a Mad2 SAC response that delays anaphase when polytenes remain at metaphase, and a SIRS response that eliminates polyteny as cells enter metaphase. Despite the lack of metaphase polytene chromosomes in papillar cells, we also identified an important role for Mad2 during SIRS. Because *mad2* loss has no reported mitotic defects in *Drosophila* animals (Buffin *et al.*, 2007), we were surprised to find that first division *mad2* papillar cells exhibit a substantial increase in DNA bridges (**FIG4A,B**). We did not detect similar defects during papillar mitosis of animals null for *mad1,* another SAC component (**Fig4A,B**). Thus, a Mad1 independent function of Mad2 is important in cells during SIRS.

In *Drosophila*, Mad2 plays a conserved, cell type-dependent role in regulating NEBD-to-anaphase onset timing (Buffin *et al.*, 2007; Meraldi *et al.*, 2004; Rodriguez-Bravo *et al.*, 2014; Yuan & O'Farrell, 2015). As for the wait-anaphase response, this mitotic timing role involves Mad2 inhibition of the Anaphase Promoting Complex. However, Mad2's control of overall mitotic timing is irrespective of SAC kinetochore attachment surveillance (Meraldi *et al.*, 2004; Rodriguez-Bravo *et al.*, 2014). Interestingly, *Drosophila* Mad1 is reported to be dispensable for regulation of NEBD-to-anaphase timing (Emre *et al.*, 2011). Given the lack of *mad1* phenotypes with respect to the first papillar division, we thus hypothesized that SIRS enables papillar cells to bypass the SAC-mediated anaphase delay, and that Mad2 control of overall mitotic timing is important during SIRS. If so, one would predict cells undergoing SIRS to not trigger an anaphase delay, but to still depend on mitotic timing.

To first test if papillar cells employ the SAC wait-anaphase in response to polytene chromosomes, we treated animals with colcemid, a known SAC wait-anaphase trigger. This treatment increases the mitotic index of wild type papillar cells, whereas the mitotic index of *mad2* null animals is unaffected (**Fig4C,D**) Thus, spindle defects trigger the SAC wait-anaphase response in papillar cells. We next asked if the SAC wait-anaphase responds to polytene chromosomes during SIRS. If so, the first divisions (polytenes present) should have a longer metaphase than the second division (polytenes absent). However we find that metaphase is not any longer in the first papillar division than in the second papillar division, while in contrast metaphase is almost twice as long in wing cells with diplochromosomes (+10hr) than in those that are polyploid but lack diplochromosomes (+24hr, **Fig4E**). We then tested if triggering the SAC wait-anaphase response can prevent or delay SIRS completion. We find SIRS occurs on schedule even in the presence of colcemid concentrations that are sufficient to eliminate a detectable spindle and inhibit

anaphase (**Fig4F,G**). We conclude that: a) SIRS is not regulated by the SAC wait-anaphase response, and b) chromosome separation during SIRS does not require a mitotic spindle.

We next tested whether Mad2-dependent control of overall mitotic timing is crucial for efficient SIRS. Using an NEBD marker, we first confirmed that Mad2 regulates NEBD-to-anaphase timing (**Fig5A,B**). We also co-imaged NEBD and kinetochores to monitor SIRS completion in wild type and *mad2* papillar cells. Interestingly, in both *mad2* and wild type animals, SIRS begins synchronously with NEBD (**Fig5C,D**)**.** However, SIRS fails to complete before anaphase in *mad2* animals*,* leading to a high variance of centromere intensity signal across the metaphase plate (reflecting failure of centromere dissociation/SIRS completion). This high variance disrupts the bilateral symmetry of the metaphase plate in *mad2* cells that form DNA bridges (**Fig5E,F**). Taken together, our data show mitotic fidelity after genome reduplication is improved by one of two Mad2-dependent functions: 1) in the presence of metaphase polytene chromosomes a Mad2 SAC dependent wait-anaphase signal is generated, 2) the efficient elimination of polytenes as cells enter metaphase by SIRS requires a Mad2 (but SAC wait-anaphase-independent) NEBD-anaphase timer (**Fig5G**).

DISCUSSION

Two Mad2 responses to genome reduplication

Despite a large body of literature describing reduplicated chromosomes in development and disease, the cellular and molecular responses enabling cells to progress through mitosis after genome reduplication have remained essentially unknown. Here, we define two such responses- one that prevents malformation of tissues with polytene chromosomes that persist until anaphase onset, and another (SIRS)

that eliminates polyteny before anaphase onset. Both polyteny responses require the conserved mitotic fidelity regulator Mad2, yet Mad2's role in each response is distinct (anaphase delay vs. control of overall mitotic timing). These findings identify new roles for *Drosophila* Mad2, for which few roles have been identified. Further, our findings illuminate a likely recurring role for Mad2 in response to genome reduplication.

In cells with metaphase polytenes (*e.g.* diplochromosomes), our data suggest polytene chromosomes present a challenge for the mitotic spindle, leading to a prolonged period of unattached/tensionless kinetochores. What particular feature of diplochromosomes triggers the SAC wait-anaphase response is unclear. It seems likely that diplochromosome structure is at least partially incompatible with attachment to the spindle. For example, it may be that the outer kinetochores block spindle attachment to the inner kinetochores within a diplochromosome, or it could be that the spindle has trouble generating tension on four kinetochores simultaneously, both of which would trigger the SAC wait-anaphase response. Eventually, the spindle appears able to attach and bi-orient all kinetochores, but the resulting anaphase is frequently error prone. These data are consistent with the known ability of cells with erroneous merotelic kinetochore attachments to satisfy the SAC and proceed to anaphase with lagging chromosomes (Gregan *et al.*, 2011), the latter of which we observe (**Fig1I**). Potentially, then, the AuroraB-mediated mechanism that can correct merotely is overwhelmed/inoperable in cells with reduplicated chromosomes (Cimini *et al.*, 2006; Knowlton *et al.*, 2006). Despite the inability of the SAC to prevent all instances of mitotic errors in cells with polyteny, our data suggest that development of normally diploid tissues with an operable SAC is not noticeably altered by up to 23% ± 4.9% of error prone tetraploid divisions. Given the conserved nature of SAC signaling, and the widespread occurrence of diplochromosomes in disease, it will be interesting to explore whether the SAC wait-anaphase response

370 is a general mechanism used to enable the expansion of aneuploid cells formed by aberrant genome
371 reduplication.

372

373 In contrast to cells with polyteny at anaphase, in cells such as papillar cells, SIRS vastly improves mitotic
374 fidelity. This process does not require the Mad2 SAC wait-anaphase response, but the efficient completion
375 of SIRS before anaphase requires the Mad2-dependent mitotic timer. Little is known about distinct,
376 checkpoint-independent regulation of the Mad2 timer. In the future, papillar cells may prove useful in
377 further study of the timer, given the dependence of SIRS completion on this Mad2 function.

378

379 We previously described the error-prone nature of papillar divisions, as well as the high tolerance of this
380 tissue for chromosome mis-segregation. This raises the question of why papillar cells employ SIRS, if
381 papillar aneuploidy is well tolerated (Schoenfelder *et al.*, 2014). Based on our study of *HS>fzr* cells, which
382 lack SIRS, we propose that SIRS is required to prevent extreme polytene chromosome mis-segregation
383 events during papillar development, which could result in inviable nullisomic cells. Additionally, we have
384 recently found that papillar cells actively prevent accumulation of micronuclei resulting from broken DNA
385 (Bretscher and Fox, unpublished). Thus, while mitotic genome-reduplicated cells such as papillar cells do
386 tolerate some degree of aneuploidy, processes such as micronucleus prevention and SIRS may act to
387 ensure a viable degree of mitotic fidelity.

388

389 **A model for SIRS**

390 Our results identify SIRS as a spindle-independent chromosome separation process that remarkably
391 eliminates polytene chromosomes before anaphase. This process is distinct from another spindle-

independent chromosome separation process known as C-mitosis, which involves complete sister chromatid separation before anaphase (Levan, 1938; Östergren, 1944). While future work will determine what differentiates cells capable of SIRS from cells with polytenes that persist until anaphase, our data thus far has examined three layers of polytene chromosome organization that either are or are not eliminated during papillar and *HS>fzr* mitosis, and has pinpointed one of these layers of polytene organization as distinct to cells undergoing SIRS.

The first layer of polytene organization is homolog-homolog pairing. Given that we observe the haploid number of chromosomes after both papillar (**Fig3B**) and HS>*fzr* (**Fig1F**) endocycles, it is clear that homologous chromosomes associate within both types of polytene chromosomes by somatic homolog pairing (Metz, 1916; Painter, 1933). Both papillar and *HS>fzr* polytenes separate homologs before dividing (**Fig3B'', Fig1F'**), and this process appears to initiate at centromeres (**Fig1F**, **Fig 3B**, asterisks, most obvious for the acrocentric X chromosome). Thus, homolog-homolog dissociation is not unique to SIRS. The second layer of polytene organization is interaction between sister chromatid pairs. Importantly, the arrangement of chromatid pairs at metaphase differs between cells that do or do not undergo SIRS. In SIRS-capable (e.g. papillar) cells, only the product of the single most recent round of replication (recent sisters, see nomenclature) remain attached at metaphase whereas the products of previous rounds of replication are no longer attached. In contrast, in SIRS-incapable (e.g. *HS>fzr*) cells, all sister chromatids remain attached. Thus, the separation into chromatid pairs appears to be the critical function of SIRS. Future work can test if this separation requires the Condensin II complex activity during SIRS, which was shown previously to enable partial polytene chromosome dissociation (Hartl *et al.*, 2008). The third layer of organization within polytenes are contacts between recent sister chromatid arms. These are equally undone by metaphase in both papillar and HS>*fzr* cells (**Fig3B'', Fig1F'**) so that, at metaphase, chromatids are only attached at the centromere. This process likely involves the prophase cohesin removal pathway (Losada *et al.*, 2002;

Sumara *et al.*, 2002). Taken together, we conclude the key difference between SIRS-capable (e.g. papillar) and SIRS-incapable (*e.g,* HS>*fzr)* cells is the ability to separate into sister chromatid pairs before metaphase (**Fig5G**).

We further hypothesize that a key prerequisite to SIRS is the careful regulation of chromosome structure during genome reduplication/endocycles. During the endocycle, papillar cells show no evidence of karyokinesis, which suggests these cells lack a mechanical method of separating chromosomes during the endocycle (Fox *et al.*, 2010). However, we speculate that during endocycles, periodic cohesin removal occurs at centromeres after each S-phase. Such cohesin removal would then allow each chromatid to both eliminate its cohesins between its sister from a previous S-phase and then establish cohesins with a new sister during the subsequent S-phase. While alterations in cohesins do not noticeably perturb interphase polytene structure (Pauli et al, 2008), future work can determine if such endocycle-mediated cohesin regulation confers cells with polytene chromosomes with the ability to undergo SIRS during a later mitosis. Future work can also determine if cohesin regulation differs during endocycles of cells that are destined to later divide. We previously defined features of a distinct pre-mitotic variant of the endocycle (Schoenfelder *et al.*, 2014), and cohesin regulation may be distinct during this endocycle variant.

SIRS is likely frequent and conserved. Consistent with classical reports (Berger, 1938; Grell, 1946; Holt, 1917), we find polytene chromosomes are present before polyploid mitosis in the ileum of the mosquito *Culex pipiens,* and are later apparent as individual chromosomes during mitosis (**FigS3E**). Polyploid *Drosophila* ovarian nurse cells undergo an incomplete SIRS-like process (Dej & Spradling, 1999), and can further separate if mitotic cyclins are experimentally elevated (Reed & Orr-Weaver, 1997). In polyploid trophoblasts of some mammalian species, polytene chromosomes separate into numerous bundles of

paired chromosomes at the polykaryocyte stage (Zybina & Zybina, 1996; Zybina *et al.*, 2011). SIRS may also act to eliminate polyteny in some polyploid tumors. One of the first descriptions of polyteny in tumors noted diplochromosomes "fall apart" before anaphase (Levan & Hauschka, 1953). Whole genome duplication is common (~37%) in human tumors (Zack *et al.*, 2013). Given the transient nature of polytene chromosomes in mitotic tissues demonstrated here, we suggest future studies of whole genome duplication in cancer models should closely examine the initial mitosis after multiple S-phases to identify potential polytene chromosome origins of tumor aneuploidy. Finally, while our studies agree with the notion that multiple S-phases and polyploidy precede aneuploidy (Davoli & de Lange, 2012; Gordon *et al.*, 2012), they also underscore the need for aneuploidy-prevention responses including SIRS and the SAC for continued propagation of viable polyploid/aneuploid cells. Future studies can reveal additional SIRS regulation, and other critical genome instability controls in normal or tumorous cells following genome reduplication.

MATERIALS AND METHODS

Drosophila genetics: All flies were raised at 25^{o} on standard media (Archon Scientific, Durham, NC). For experiments to measure the length of mitosis larvae or pupae were shifted to 29^{o} for at least 18 hrs before dissection. Heat shocks were performed on third instar larvae. Vials were heat shocked in a 37^{o} water bath for 15min, 30min, or 60min. Flybase (flybase.org) describes full genotypes for the following stocks used in this study: *engrailed Gal4* (Bloomington stock 1973); w^{1118} (Bloomington stock 3605); *His-2av-GFP* (Bloomington stock 24163); *UAS>GFP.E2f1.1-230, UAS>mRFP1.CycB.1-266* (Bloomington stock 55117). Kyoto DGRC (kyotofly.kit.jp) describes the genotype for the following stock: S/G2/M-Azami (Kyoto stock 109678). The Other stocks were generous gifts: *tomato-Cenp-C* (Althoff *et al.*, 2012); *HS>fzr* (Sigrist & Lehner, 1997); *byn>gal4* (Singer *et al.*, 1996); $mad1^{1}$*, Df (2R) W45-30n* (Emre *et al.*, 2011);

462 *mad2*^{p} (Buffin *et al.*, 2007), *msl3-GFP* (Strukov *et al.*, 2011), *stg>LacZ*$^{4.9}$ (Bruce Edgar), *jupiter-GFP*
463 (Karpova *et al.*, 2006).

464

465 *Mosquito culture: Culex pipiens* larvae were obtained from Carolina Biological (Burlington, NC). Culturing
466 conditions were as in Fox *et. al,* 2010. Larvae were monitored hourly for pupation, and the hindgut was
467 dissected beginning 7 hours post-puparium formation. Antibody staining was as for *Drosophila* tissue.

468

469 *Survival analysis:* 20 wandering 3rd instar larvae per replicate of the indicated genotype were placed into
470 a fresh vial with food and then heat shocked for 15 or 30 minutes. The number of adults that eclosed
471 was counted.

472

473 *Chromosome Cytology and FISH:* Chromosome preparations were based on previous protocols with
474 modifications for the pupal hindgut (Fox *et al.*, 2010; Gatti *et al.*, 1994). For colcemid treatment to
475 enrich for metaphase cells tissue was first incubated in colcemid (Sigma, St. Louis, MO) at 50µg/ml for
476 30min in PBS. For pre-mitotic chromosome spreads with Premature Chromosome Compaction, tissue
477 was incubated in Calyculin A (Cell Signaling Technology, Danvers, MA) at 200nM in PBS for 30min,
478 (Gotoh *et al.*, 1995; Miura & Blakely, 2011). FISH was performed as in Dej & Spradling, 1999. BAC clone
479 #BACN04H23 (Chromosome 3L, region 69C3-C8) from the PacMan collection (Venken *et al.*, 2006) was
480 labeled using the BioNick labeling system (Invitrogen, Carlsbad, CA). BAC probe signal was amplified
481 through sequential labeling with Peroxidase-labeled Streptavidin followed by the TSA Peroxidase
482 detection kit (Perkin Elmer, Waltham, MA). Imaging was performed on a Zeiss Axio Imager 2 with a 63x
483 oil immersion lens.

Live Imaging: Tissue was dissected and cultured based on previous protocols with modifications for the pupal hindgut (Fox *et al.*, 2010; Prasad *et al.*, 2007). For colcemid live imaging experiments, pupae were dissected and imaged in media containing 50µg/ml of colcemid (Sigma), from the initiation of dissection to the first frame was at least 15 minutes and up to 1 hour. Imaging was performed on a spinning disc confocal (Yokogawa CSU10 scanhead) on an Olympus IX-70 inverted microscope using a 60x/1.3 NA UPlanSApo Silicon oil, 100x/1.4 NA U PlanSApo oil, or a 40x/1.3 NA UPlanFl N Oil objective, a 488 nm and 568 nm Kr-Ar laser lines for excitation and an Andor Ixon3 897 512 EMCCD camera. The system was controlled by MetaMorph 7.7.

Fixed Imaging: Tissue was dissected in PBS and immediately fixed in 3.7% formaldehyde + 0.3% Triton-X for 15 minutes. Immunostaining was performed in 0.3% Triton-X with 1% normal goat serum as in Fox *et al.,* 2010. The Fluorescent Ubiquitination-based Cell Cycle Indicator (FUCCI) probes (Zielke *et al.*, 2014) and mouse anti-Phospho-Histone H3 (ser 10) (Cell Signaling Technology, 1:1000) were used to determine cell cycle stages. Rabbit anti-RFP (MBL, Woburn, MA, 1:500) was used to detect Cenp-C-Tomato Foci. Rabbit anti-DCP1 (Cell Signaling Technology), 1:500 was used to measure cleaved caspases. TUNEL staining was performed with the *in situ* cell death detection kit (Roche, Basel, Switzerland) according to the protocol in Schoenfelder *et al.,* 2014. Tissue was stained with DAPI at 5µg/ml. Images were obtained using a Leica SP5 inverted confocal with a 40x oil objective. Emission was done using a 405nm diode laser, an argon laser tuned to 488nm emission, a 561nm Diode laser, and a 633 HeNe laser.

Image Analysis: All image analysis was performed using ImageJ (Schneider *et al.*, 2012). nuclear envelope brightness was calculated by measuring Geminin-Azami intensity or a single cell. The brightness for each cell was normalized from 1 to 0, with 1 being the highest pixel intensity value and 0 being the dimmest value for a single cell across all time-points. Anaphase was determined as the first frame with poleward movement of the kinetochores as evident by Cenp-C-Tomato. Time from NEBD to anaphase was determined as the point from half-maximal Azami signal to anaphase. To calculate kinetochore clustering we closely cropped around the cell of interest for all frames. We then used a thresholding approach to outline each centromere or group of centromeres and stored those as ROIs. We then used those ROIs to measure the average intensity of each centromere pixel and the total area of all the pixels. We reasoned that as centromeres disperse the total area they cover increases and there is a corresponding decrease in fluorescence intensity from each individual point, therefore we divided the average pixel intensity by the area and normalized that on a scale from 1 to 0. To measure symmetry of metaphase centromere alignment (**Fig5E-F**), we generated a line plot of each metaphase plate at the frame immediately prior to metaphase. We then generated aggregate plots of each genotype.

Nomenclature: For chromosomes we use “homolog” to distinguish maternally and paternally contributed chromosomes of the same chromosome type. All chromatids of the same homolog are considered “sisters.” We use “recent sister” to refer to two chromatids that are the product of the most recent S-phase. “Polytene” refers to the chromosome state of any cell formed by genome reduplication that has not fully separated its chromosomes into recent sisters. 4 chromatids conjoined at centromeres are “diplochromosomes”. 8 chromatids conjoined at centromeres are “quadruplochromosomes”. We use the term “endocycle” to refer to any cell cycle involving successive genome reduplication without any sign of M-phase. We note the use in the literature of terms such as “endoreduplication”, “re-replication”, and “endoreplication” to often refer to the same phenomenon.

530

531

532 ACKNOWLEDGMENTS

533 The following kindly provided reagents used in this study: The Bloomington Stock Center, the Vienna
534 /Drosophila Resource Center, the Kyoto Drosophila Genetic Resource Center, Roger Karess (U. Paris),
535 Christian Lehner (U. Zurich), Mitzi Kuroda (Harvard University), and Bill Sullivan (U.C. Santa Cruz). We
536 thank David MacAlpine, Eda Yildirim, Beth Sullivan, Joshua Bembenek, and Fox lab members for valuable
537 comments on the manuscript. Work on polyploidy in the Fox lab is supported by a Pew Scholar Award,
538 (Pew Charitable Trusts), a Basil O' Connor Scholar Award (The March of Dimes) a Whitehead Scholar
539 Award (Whitehead Foundation), and Scientist Development Award (American Heart Association), and a
540 Creative and Novel Ideas in HIV Research Award (NIH Centers For AIDS Research/International AIDS
541 Society).

542

543 FIGURE LEGENDS

544 Figure 1) Induced genome reduplication in wing progenitors leads to polytene diplochromosomes and
545 aneuploidy.

546 A) A model for the cell cycle progression following *fizzy-related (HS>fzr)* over expression in a
547 mitotically cycling tissue. Cells progress directly from G2 into G1 without an intervening mitosis,
548 resulting in an additional S-phase.

549 B) A diagram depicting the Fly-FUCCI system in each stage of the cell cycle, and representative
550 images of wing imaginal disc cells in each cell cycle state. GFP-E2F1$_{1-230}$ (green) is nuclear during
551 G1 and G2 and fills the cell during mitosis. RFP-CycB$_{1-266}$ (magenta) is cytoplasmic during S-phase
552 and G2 and fills the cell during mitosis.

553 C) Representative micrographs of the wing imaginal disc pouch expressing UAS Fly-FUCCI under the
554 control of *engrailed-Gal4* in the absence of *HS>fzr* expression (No HS, C) as well as +2hrs (C') and
555 +10hrs (C'') after a 60 minute heat shock to induce *HS>fzr* expression. GFP-E2F1$_{1-230}$ is in green,
556 RFP-CycB$_{1-266}$ is in magenta.

557 D) The percentage of cells in G1, S, G2, and M based on Fly-FUCCI expression prior to *HS>fzr*
558 expression (No HS), +2hrs and +10hrs after expression. Stacked bars represent mean plus
559 standard error of the mean (+S.E.M.), ***= $p < 0.001$, NS = $p > 0.05$, t-test. Data are an average of
560 three replicates with at least 5 animals per replicate and at least 50 cells counted per animal.

561 E) Representative karyotypes from a mitotic *HS>fzr* wing imaginal disc cells without heat shock.
562 Chromosomes are pseudocolored according to each chromosome type and numbered. Prior to
563 *HS>fzr* expression cells display a normal diploid karyotype. Tissue was incubated in colcemid for
564 30min to enrich for mitotic cells.

565 F) Representative karyotypes from mitotic *HS>fzr* wing imaginal cells 10hrs after heat shock.
566 Chromosomes are pseudocolored according to the type as in Fig1E. Transiently, closely aligned

polytene chromosomes are seen when chromosomes first condense after genome reduplication (F). Asterisks indicate the 2 groups of homologous centromeres of the X-chromosome. Diplochromosomes, characterized by the attachment of four centromeres of each sister chromatid (F' see inset), are seen at the first metaphase after genome reduplication. Tissue was incubated in colcemid for 30min to enrich for mitotic cells.

G) Representative karyotype of a mitotic *HS>fzr* cell 24hrs after heat shock, colored according to type as in Fig1E. Aneuploid cells are observed at 24hrs after heat shock, during the second metaphase after genome reduplication, which follows the division of diplochromosomes. Tissue was incubated in colcemid for 30min to enrich for mitotic cells.

H) The percentage of wing imaginal disc karyotypes classified as euploid/diploid, euploid/tetraploid, euploid/diplo-tetraploid, or aneuploid/tetraploid prior to heat shock (No HS), or +10hr, +24hr, or +120hr after heat shock. Stacked bars represent Mean (+S.E.M.), *** = $p < 0.001$, NS = $p > 0.05$, t-test. Data are an average of 3 replicates with at least 50 karyotypes per replicate.

I) Representative time-lapse of a diploid wing imaginal disc cell dividing prior to *HS>fzr* expression (No HS) and a tetraploid cell with diplochromosomes dividing 10hr after *HS>fzr* expression (HS +10hr). Yellow arrowhead shows a single lagging kinetochore. Red arrows highlight a single diplochromosome that segregates its chromatids in a 3:1 fashion. Cenp-C-Tomato showing kinetochores in cyan, His2av-GFP showing DNA in magenta. Time represents minutes from the last frame prior to anaphase.

J) The percentage of lagging chromosomes in diploid cells, in tetraploid cells with diplochromosomes (4N Diplo), and in tetraploid cells without diplochromosomes (4N) after *HS>fzr* expression. Bars represent averages (+S.E.M.) between animals with at least five animals per condition. *** = $p < 0.001$, NS = $p > 0.05$, t-test.

K) A model for a cell cycle that results in aneuploid daughter cells showing only the two homologs of a single chromosome for simplicity. The two homologs are shown in black and gray with a red centromere. Chromatids are replicated in S-phase and then reduplicated following a heat shocked induced endocycle. This results in polytene chromosomes. Diplochromosomes are seen as the genome-reduplicated cells progress into metaphase. At anaphase, diplochromosome segregation frequently produces lagging chromatids, which can segregate erroneously resulting in aneuploidy.

Scale bars represent 5μm, except in inset in F' and G where it represents 1μm.

Figure 2) The spindle assembly checkpoint wait-anaphase response is required after ectopic genome reduplication.

A) Quantitation of survival rates from third instar larvae to adulthood of the indicated genotypes without heat shock (dark blue) or following a 15min heat shock (light red) (which generates 23% tetraploid, see methods). Bars represent means + standard error of the mean (S.E.M) of at least 5 independent experiments, with 20 animals per experiment. * = $p < 0.05$, *** = $p < 0.001$, NS = $p > 0.05$, t-test.

B) Representative micrographs of eyes, wings, and abdomens from *HS>fzr* alone, *mad2* alone, or *HS>fzr*, *mad2* flies heat shocked as third instar larvae and then allowed to develop to adults. Red arrow indicates an extra ectopic wing vein, and yellow arrow heads indicate melanotic masses both of which are found in in *HS>fzr, mad2* adults following heat shock.

C) Representative time-lapse showing a *hs>fzr* wing imaginal disc including a cell with diplochromosomes (yellow dotted line) and a diploid cell (blue dashed line) dividing within the same field (one of the diploid daughters drifts vertically out of the frame). The cell with

613 diplochromosomes takes more than four times as long to enter anaphase, and division is error
614 prone. His2av-GFP showing DNA is in white. Time indicates minutes from the start of filming.
615 D) The length of metaphase without *fzr* overexpression (No HS) or +10hr after overexpression from
616 *HS>fzr,* and *HS>fzr, mad2* larval wing imaginal disc cells. Points represent individual cell
617 divisions, bars represent means, diploid cells are represented in dark blue, polyploid cells are
618 represented in light red, *HS>fzr* is represented in circles, *HS>fzr, mad2* is represented in
619 triangles. N>35 cells per condition. ** = $p < 0.01$, *** = $p < 0.001$, Not Significant (NS) = $p > 0.05$,
620 ANOVA.
621 E) Third instar larval wing imaginal discs from HS>*fzr* or HS>*fzr, mad2* stained for TUNEL in green
622 and DAPI in magenta without heat shock (No HS) or +24hr after a 15min heat shock.
623 F) Quantification of the number of TUNEL positive foci per wing disc for *HS>fzr* and *HS>fzr, mad2*
624 without heat shock (No HS, blue bars) or 24hrs after a 15min heat shock (+HS, red bars). Points
625 represent individual wing imaginal discs, bars represent mean, N ≥ 18 discs per condition. NS = p
626 > 0.05, * = p <0.05, *** = p <0.001, ANOVA.
627 Scale bars represent 500μm in B, 5μm in C, and 50μm in E.

628

629 Figure 3) Programed genome reduplication in papillar cells is followed by Separation Into Recent Sisters
630 (SIRS), which eliminates polytene chromosomes.

631 A) A model of the cell cycles in *Drosophila* papillar cells. These cells undergo two rounds of the
632 endocycle in the 2nd instar to reach 8N/16C, then enter a G2-like state, then undergo, on average,
633 two cell divisions with intervening S-phases during pupation (Fox *et al.*, 2010; Schoenfelder *et al.*,
634 2014).

B) Karyotypes of papillar cells during the 1st polyploid division, (B-B''). Chromosomes are pseudocolored according to type and labeled in panel B. Panel B inset shows the 4th chromosomes, which were out of frame. When chromosomes first condense following genome reduplication, they are in a polytene configuration (asterisks indicate the 8 separated centromere pairs of an otherwise polytene X chromosome). B' Example of the clumped configuration in early mitosis of the first papillar division. B'' Example of fully separated 1st division papillar chromosomes. No diplochromosomes are present (compare X chromosome in inset to inset in Fig1F').

C) Karotype of papillar chromosomes during the 2nd polyploid division. Chromosomes are pseudocolored according to type as in Fig3B. At the second division almost all cells show chromosomes fully separated into sister pairs.

D) Percentage of cells with polytene chromosomes, recent sisters clumped, or recent sisters clearly separated from four time points: prior to the first division (following treatment with Calyculin A to visualize pre-mitotic chromosome structure- see Methods), during the first division (no drug treatment), during the first division (following treatment for 30min with colcemid to enrich for late metaphase (1st Div + colc)), and during the second division (no drug treatment). * = $p < 0.05$ compared to 1st Division, chi-squared test, $N \geq 26$ karyotypes per treatment.

E) Quantification of the number of resolvable Cenp-C-Tomato foci in fixed papillar cells during the course of pupation (expressed in hours post pupation). Before the first mitosis (18hr) each cell has an average of 4.1 kinetochore foci closely corresponding to the haploid chromosome number, following the first division (24hrs) cells average 15.1 foci per cell. At 20hr some cells have divided and others are yet to divide and the distribution is bimodal. Circles represent individual cells. Bars represent the mean of 3 animals per time point and 15 cells per animal.

F) Live imaging of the 1st divisions from wild type papillar cells shows the SIRS process. Cenp-C-Tomato (Cenp-C) is in cyan, His2av-GFP (His) is in magenta. Time represents minutes to the last frame prior

659 to anaphase. In the 1st division kinetochores from a group of homologs are tightly clustered prior to
660 division. At -18:00 min. relative to anaphase, chromosome condensation has begun and polytene
661 chromosomes are visible (See His channel). Dispersal continues until individual pairs of sister
662 kinetochores are evident at metaphase. The inset shows the Cenp-C-Tomato channel of a single
663 kinetochore focus from time frames -36min to -8min.
664 G) Live imaging of the 2nd division from a wild type papillar cell. In contrast to the first division many
665 discrete kinetochore foci are evident at time-points prior to the onset of mitosis, and polytene
666 chromosomes are never evident.
667 H) A model for a pair of homologs undergoing 2 rounds of endo-S-phase to become a polytene 16C
668 chromosome. The polytene chromosome then separates into pairs composed of only the most
669 recent sister chromatids during mitosis, and each sister then segregates to opposite poles at
670 anaphase.
671 Scale bar represents 5 μm, except in insets in B'' and F where it represents 1μm.

672

673 Figure 4) SIRS does not depend on the SAC wait-anaphase response or formation of a mitotic spindle.

674 A) Representative micrographs of wild type (WT), *mad2,* and *mad1* cells 1st divisions beginning in
675 the last frame of metaphase (0:00) and continuing through eight minutes of anaphase. Cenp-C-
676 Tomato showing kinetochores in cyan, His2av-GFP showing DNA in magenta. Yellow arrowheads
677 show kinetochores that are part of a bridge between the two poles in a *mad2* cell. Time
678 represents minutes from the last frame prior to anaphase.
679 B) Quantification of the frequency of persistent DNA bridging observed 4 min after the onset of the
680 1st division anaphase from papillar cells in wild type (WT), *mad2,* and *mad1* animals. Bars

represent the mean of all cell divisions, + Standard Error of the Mean (S.E.M.) ***=p < 0.001, t-test.

C) Representative images of a single pupal rectums from wild type or *mad2* animals treated with colcemid for 60min prior to fixation and stained for Phospho-Histone H3 (PH3) positive nuclei in magneta and expressing GFP under the control of *brachyenteron (byn,* a hindgut marker) in green.

D) The fold increase in the number of polyploid mitotic cells per hindgut from wild type and *mad2* animals following treatment with colcemid compared to without colcemid. A value of 1 equals no difference. Bars represent mean fold change (+ SEM), and are labeled with the mean value. ** = p < 0.01, t-test.

E) The fold increase in metaphase length for *HS>fzr* polyploid cells with (1^{st}) and without polytene diplochromosomes (2^{nd}) compared to papillar cells with (1^{st} division) and without (2^{nd} division) polytene chromosomes. A value of one equals no difference between 1^{st} and 2^{nd} divisions. The increase in *HS>fzr* wing cells indicates that metaphase polytene diplochromosomes trigger the spindle assembly checkpoint. Bars represent means (+SEM), and are labeled with the mean value. ** = p <0.01, t-test.

F) Live imaging of a cell expressing Cenp-C-Tomato in cyan and Jupiter-GFP in magenta undergoing SIRS in the presence of a vehicle control. Time represent minutes before the onset of SIRS. Inset shows the dispersal of a single Cenp-C-Tomato kinetochore at all the time points between 0min and 16min. F') shows the number of resolvable Cenp-C-Tomato foci from prior to SIRS (0 min) and after SIRS (16 min), points represent individual cells with the two time points connected by a line. *** = p < 0.001, t-test.

G) Live imaging of a cell expressing Cenp-C-Tomato in cyan and Jupiter-GFP in magenta undergoing SIRS in the presence of a colcemid. Time represent minutes from the onset of SIRS. Inset shows

the dispersal of a single Cenp-C-Tomato kinetochore at all the time points between 0min and 16min. G') shows the number of resolvable Cenp-C-Tomato foci from prior to SIRS (0 min) and after SIRS (16 min), points represent individual cells with the two time points connected by a line. *** = $p < 0.001$, t-test.

Scale bar represents 5μm except in insets of F and G where they represent 1μm.

Figure 5) SIRS is dependent on Mad2-dependent mitotic timing

A) Live imaging of a representative wild type and *mad2* cell expressing geminin-Azami (to highlight nuclear envelope integrity) in magenta and Cenp-C-Tomato (to highlight kinetochores) in cyan during the 1st papillar division. Nuclear Envelope Breakdown (NEBD) can be seen when the geminin signal goes from nuclear to cytoplasmic. Time represents minutes from NEBD. Yellow cross hatch represents the frames during which the cell is in mitosis. The *mad2* cell takes less time from NEBD to anaphase.

B) The length of time from NEBD to anaphase in wild type and *mad2* papillar cells. Points represent individual cell divisions. *** = $p < 0.001$, t-test.

C) Live imaging of the initiation of SIRS and the period of NEBD with Cenp-C-Tomato in cyan and Geminin-Azami in magenta. Time represents minutes prior to the start of anaphase.

D) Quantification of the intensity of geminin-Azami in magenta and a measure of kinetochore clusteredness in cyan over time with 0 minutes representing the onset of anaphase. Both measures decline synchronously at the onset of NEBD. Data represents the mean of 22 cells.

E) Representative images of Cenp-C-Tomato forming the metaphase plate of WT or *mad2* cells immediately prior to the onset of anaphase with reds indicating more Cenp-C-Tomato signal and blue indicating less signal (Top) and line graphs measuring the total signal intensity from left to

right (Bottom), in call cases the eventual division is in the same left-right orientation. *mad2* metaphases were split into those that did not generate a persistent DNA bridge at anaphase (no bridge) and those that did (persistent bridge).

F) Aggregate plots of the line graph and the confidence interval for each category in E. *mad2* with bridging is significantly more variable than Wild Type or *mad2* without bridging. N > 13 cells per category.

G) Model: A simplified model in which a four sisters from a single round of genome reduplication are shown. In cells with SIRS (down arrow) polytenes fully split into individual sister pairs and with a functioning mitotic timer complete SIRS and divide evenly. However, in the absence of the timer anaphase is precocious and DNA bridges result from incompletely resolved polytene chromosomes. In cells without SIRS (upper arrow), diplochromosomes result. The spindle assembly checkpoint (SAC) delays cells in metaphase and reduces but does not eliminate aneuploidy during the ensuing anaphase. In the absence of a checkpoint, cell death results from errant diplochromosome divisions.

SUPPLEMENTAL MATERIAL

Supplemental Figure Legends

Figure S1) Supporting data regarding the effect of *HS>fzr* on imaginal discs and brains.

A) Representative micrographs of 3rd instar wing imaginal discs from *HS>fzr* animals stained for Phospho-HistoneH3 (PH3, green) and DAPI (magenta) prior to heat shock (No HS, A) as well as +2hr (A') and +10hr (A'') after heat shock.

B) Bee-swarm plot depicting the number of Phospho-HistoneH3 (PH3) positive cells per animal prior to heat shock (No HS), immediately after heat shock (2-7 hours post) or 10 hours post heat shock for *HS>fzr* (dark blue circles) and wild type (w^{1118}, light blue triangles). N ≥ 6 animals per time point.

C) The proportion of 3rd instar larval brain karyotypes prior to heat shock (No HS), or +10hr, +24hr and +120hrs after heat shock, classified as euploid/diploid, euploid/polyploid, euploid/diplo-polyploid, or aneuploid/polyploid. Stacked bars represent Mean + Standard Error of the Mean (+S.E.M.), ** = $p < 0.01$, *** = $p < 0.001$, t-test, data are an average of 3 replicates with at least 50 karyotypes per replicate.

D) The proportion of aneuploidies caused by 3:1 non-disjunction or 4:0 non-disjunction of wing imaginal disc diplochromosome divisions, inferred from subsequent divisions. Information is divided into gains and losses. N = 52 aneuploidies.

E) Representative time-lapse of a tetraploid cell without diplochromosomes dividing 24hrs after *HS>fzr* expression. Cenp-C-Tomato showing kinetochores in cyan, His2av-GFP showing DNA in magenta. Time represents minutes from the last frame prior to anaphase.

Scale bars represent 50 μm in A and 5μm in E.

Figure S2) Supporting data regarding Mad2's role in response to diplochromosomes.

A) Graph of the survival rate from third instar larvae to adulthood following a 30min heat shock from wild type, *HS>fzr* alone, *mad2* alone, or *HS>fzr, mad2* animals. Bars represent means + Standard Error of the Mean (+ SEM) of at least 5 experiments with 20 animals per experiment.

B) Graph showing the number of Phospho-Histone H3 positive (PH3+) cells per wing imaginal disc incubated in PBS for one hour with (+) or without (-) colcemid from wild type, or *mad2 a*nimals.

C) Micrographs of antibody staining against *Drosophila* cleaved caspase 1 protein (DCP1) in the wing disc pouch of *HS>fzr* or *HS>fzr, mad2* animals 24 hours after a 15 minute heat shock. DCP1 is in green and DAPI is in magenta. Scale bar represents 50 μm.

D) Quantification of the relative amount of DCP1 staining per wing disc normalized so that the mean of HS>fzr without heat shock (No HS) was equal to 1. Points represent individual wing discs, bars represent means with (dark blue) or without (light red) a 15 minute heat shock. * = $p < 0.05$, *** = $p < 0.001$, ANOVA.

Figure S3) Supporting data regarding SIRS.

A) Representative micrograph of the hindgut including the ileum (anterior, left) and rectum (posterior, right) stained for GFP driven by *brachyenteron (byn)* (green), *stg>LacZ*$^{4.9}$ (magenta), and DAPI (white) at 16hr post pupation, a time point shortly before the onset of the first papillar mitosis. The rectum but the not ileum stains strongly for expression of the G2/M regulator *string*.

B) Two representative micrographs taken from the same field showing Fluorescent *in situ* hybridization (FISH) to a single region on the left arm of chromosome 3 in green and DAPI in magenta during the 1st papillar division, at a time-point in which some cells have a pre-SIRS

chromosome configuration (B) while others have undergone SIRS (B'). Yellow arrowheads indicate FISH foci.

C) Karyotypes of papillar cells from just prior to the first papillar division treated with 200nM Calyculin A to induce Premature Chromosome Compaction (PCC), showing polytene chromosome organization in the interphase prior to SIRS. Asterisks indicate where the 8 recent sister chromatid pairs of the acrocentric X-chromosome have already separated into eight pairs of recent sister centromeres.

D) Live imaging of a papillar cell 1st division from a male expressing MSL3-GFP (magenta) and Cenp-C-Tomato (Cyan). MSL3-GFP is specific to the male X chromosome and only a single Cenp-C-Tomato focus is MSL3-GFP positive prior to SIRS (yellow arrows) indicating that each Cenp-C foci is composed of a single homolog. Time represents minutes prior to the final frame of metaphase.

E) Micrographs of polyploid pupal division mitotic chromosomes stained with Phospho-Histone H3 (white) from the ileum of *Culex pipiens,* showing cells in all stages of mitosis including an apparent pre-SIRS polytene phase (E), as well as a post SIRS prophase (E') cell.

Scale bars represent 5μm except in A where it represents 50μm.

Supplemental Movies

Supplemental Movie for Figure 1)

A) Movie from Figure 1I showing His2av-GFP in magenta, and Cenp-C-Tomato in cyan from a diploid HS>*fzr* wing imaginal disc cell dividing prior to *HS>fzr* expression.

B) Movie from Figure 1I showing His2av-GFP in magenta, and Cenp-C-Tomato in cyan from a teteraploid *HS>fzr* wing imaginal disc cell with diplochromosomes 10hr after *HS>fzr* expression.

C) Movie from Figure S1E showing His2av-GFP in magenta, and Cenp-C-Tomato in cyan from a tetraploid *HS>fzr* wing imaginal disc cell without diplochromosomes 24hr after *fzr* overexpression.

Time Indicates minutes to the last frame of metaphase, scale bars represent 5μm.

Supplemental Movie for Figure 2)

A) Movie from Figure 2C showing His2av-GFP from a *HS>fzr* animal 10hr after heat shock with mitosis by a polyploid diplochromosome-containing wing imaginal disc cell (yellow dotted line) and a diploid cell (blue dotted and dashed line) in the same field.

Time Indicates minutes from the start of filming, scale bars represent 5μm.

Supplemental Movie for Figure 3)

A) Movie from Figure 3F showing His2av-GFP in magenta, and Cenp-C-Tomato in cyan from a papillar cell undergoing a first division, including the SIRS process.

B) Movie from Figure 3G showing His2av-GFP in magenta, and Cenp-C-Tomato in cyan from a papillar cell undergoing a second division.

C) Movie from Figure S3D showing MSL3-GFP in magenta and Cenp-C-Tomato in cyan from a male papillar cell undergoing a first division.

D) Movie from Figure S3E' and S3E'' showing sequential z-planes from a fixed ileum of *Culex* pipiens with mitotic cells that are pre-SIRS and a post-SIRS.

Time Indicates minutes to the last frame of metaphase, scale bars represent 5μm.

Supplemental Movie for Figure 4)

A) Movie From Figure 4A showing His2av-GFP in magenta, and Cenp-C-Tomato in cyan from a wild type papillar cell during anaphase of the first mitosis.

B) Movie From Figure 4A showing His2av-GFP in magenta, and Cenp-C-Tomato in cyan from a *mad2* papillar cell from DNA condensation through anaphase of the first mitosis, including formation of a DNA bridge.

C) Movie From Figure 4A showing His2av-GFP in magenta, and Cenp-C-Tomato in cyan from a *mad1* papillar cell during from DNA condensation through anaphase of the first mitosis.

D) Movie from Figure 4F showing Jupiter-GFP in magenta and Cenp-C-Tomato in cyan from a first division papillar cell undergoing SIRS in the presence of a vehicle control.

E) Movie from Figure 4F showing Jupiter-GFP in magenta and Cenp-C-Tomato in cyan from a first division papillar cell undergoing SIRS in the presence of a colcemid.

Supplemental Movies for Figure 5)

A) Movie From Figure 5A showing Geminin-Azami in magenta, and Cenp-C-Tomato in cyan from a wild type papillar cell from prior to Nuclear Envelope Breakdown through anaphase.

B) Movie From Figure 5A showing Cenp-C-Tomato in cyan and Geminin-Azami in magenta from a *mad2* papillar cell from prior to NEBD through anaphase.

Time indicates minutes from the first frame after NEBD. Scale bar represents 5μm

857

858 **REFERENCES**

859 Althoff, F., Karess, R. E., & Lehner, C. F. (2012). Spindle checkpoint-independent inhibition of mitotic
860 chromosome segregation by Drosophila Mps1. *Mol Biol Cell, 23*(12), 2275-2291.
861 Berger, C. A. (1938). Multiplication and reduction of somatic chromosome groups as a regular
862 developmental process in the mosquito, Culex pipiens. *Contributions to embryology., 27*(167).
863 Biesele, J., & Poyner, H. (1943). Polytene Chromosomes in Two Mammary Carcinomas of the Human
864 Subject. *Cancer Research, 3*, 779-783.
865 Buffin, E., Emre, D., & Karess, R. E. (2007). Flies without a spindle checkpoint. *Nature Cell Biology, 9*(5),
866 565-572.
867 Cantero, G., Campanella, C., Mateos, S., & Cortés, F. (2006). Topoisomerase II inhibition and high yield of
868 endoreduplication induced by the flavonoids luteolin and quercetin. *Mutagenesis, 21*(5), 321-
869 325.
870 Cimini, D., Wan, X., Hirel, C. B., & Salmon, E. D. (2006). Aurora Kinase Promotes Turnover of Kinetochore
871 Microtubules to Reduce Chromosome Segregation Errors. *Current Biology, 16*(17), 1711-1718.
872 Conrad, T., & Akhtar, A. (2012). Dosage compensation in Drosophila melanogaster: epigenetic fine-
873 tuning of chromosome-wide transcription. *Nature Reviews Genetics, 13*(2), 123-134.
874 Davoli, T., & de Lange, T. (2012). Telomere-Driven Tetraploidization Occurs in Human Cells Undergoing
875 Crisis and Promotes Transformation of Mouse Cells. *Cancer Cell, 21*(6), 765-776.
876 Davoli, T., Denchi, E. L., & de Lange, T. (2010). Persistent telomere damage induces bypass of mitosis and
877 tetraploidy. *Cell, 141*(1), 81-93.
878 Dej, K. J., & Spradling, A. C. (1999). The endocycle controls nurse cell polytene chromosome structure
879 during Drosophila oogenesis. *Development, 126*(2), 293-303.
880 Edgar, B. A., & Orr-Weaver, T. L. (2001). Endoreplication cell cycles: more for less. *Cell, 105*(3), 297-306.
881 Edgar, B. A., Zieike, N., & Gutierrez, C. (2014). Endocycles: a recurrent evolutionary innovation for post-
882 mitotic cell growth. *Nature Reviews Molecular Cell Biology, 15*, 197-210.
883 Emre, D., Terracol, R., Poncet, A., Rahmani, Z., & Karess, R. E. (2011). A mitotic role for Mad1 beyond the
884 spindle checkpoint. *Journal of Cell Science, 124*(10), 1664-1671.
885 Erenpreisa, J., S. Cragg, M., Salmina, K., Hausmann, M., & Scherthan, H. (2009). The role of meiotic
886 cohesin REC8 in chromosome segregation in γ irradiation-induced endopolyploid tumour cells.
887 *Experimental Cell Research, 315*(15), 2593-2603.
888 Fox, D. T., & Duronio, R. J. (2013). Endoreplication and polyploidy: insights into development and
889 disease. *Development, 140*(1), 3-12.
890 Fox, D. T., Gall, J. G., & Spradling, A. C. (2010). Error-prone polyploid mitosis during normal Drosophila
891 development. *Genes Dev, 24*(20), 2294-2302.
892 Gatti, M., Bonaccorsi, S., & Pimpinelli, S. (1994). Chapter 21 Looking at Drosophila Mitotic
893 Chromosomes. In S. B. G. Lawrence & A. F. Eric (Eds.), *Methods in Cell Biology* (Vol. Volume 44,
894 pp. 371-391): Academic Press.
895 Gordon, D. J., Pellman, D., & Resio, B. (2012). Causes and consequences of aneuploidy in cancer. *Nature*
896 *Reviews Genetics, 13*, 189-203.
897 Gotoh, E., Asakawa, Y., & Kosaka, H. (1995). Inhibition of protein serine/threonine phosphatases directly
898 induces premature chromosome condensation in mammalian somatic cells. *Biomedical*
899 *Research, 16*, 63-68.
900 Goyanes, V., & Schvartzman, J. B. (1981). Insights on diplochromosome structure and behaviour.
901 *Chromosoma, 83*(1), 93-102.

902 Gregan, J., Polakova, S., Zhang, L., Tolić-Nørrelykke, I. M., & Cimini, D. (2011). Merotelic kinetochore
903 attachment: causes and effects. *Trends in Cell Biology, 21*(6), 374-381.
904 Grell, M. (1946). Cytological Studies In Culex I. Somatic Reduction Divisions. *Genetics, 31*(60), 60-76.
905 Hartl, T. A., Smith, H. F., & Bosco, G. (2008). Chromosome Alignment and Transvection Are Antagonized
906 by Condensin II. *Science, 322*(5906), 1384-1387.
907 Holt, C. M. (1917). Multiple complexes in the alimentary tract of Culex pipiens. *Journal of Morphology,*
908 *29*(2), 607-627.
909 Karpova, N., Bobinnec, Y., Fouix, S., Huitorel, P., & Debec, A. (2006). Jupiter, a new Drosophila protein
910 associated with microtubules. *Cell Motility and the Cytoskeleton, 63*(5), 301-312.
911 Knowlton, A. L., Lan, W., & Stukenberg, P. T. (2006). Aurora B Is Enriched at Merotelic Attachment Sites,
912 Where It Regulates MCAK. *Current Biology, 16*(17), 1705-1710.
913 Larson-Rabin, Z., Li, Z., Masson, P. H., & Day, C. D. (2008). FZR2/CCS52A1 Expression Is a Determinant of
914 Endoreduplication and Cell Expansion in Arabidopsis. *Plant Physiology, 149*(2), 874-884.
915 Levan, A. (1938). The Effect Of Colchicine On Root Mitoses In Allium. *Hereditas, 24*(4), 471-486.
916 Levan, A., & Hauschka, T. S. (1953). Endomitotic Reduplication Mechanisms in Ascites Tumors of the
917 Mouse. *Journal of the National Cancer Institute, 14*(1), 1-43.
918 London, N., & Biggins, S. (2014). Signalling dynamics in the spindle checkpoint response. *Nature Reviews*
919 *Molecular Cell Biology, 15*(11), 736-748.
920 Losada, A., Hirano, M., & Hirano, T. (2002). Cohesin release is required for sister chromatid resolution,
921 but not for condensin-mediated compaction, at the onset of mitosis. *Genes Dev, 16*(23), 3004-
922 3016.
923 Meraldi, P., Draviam, V. M., & Sorger, P. K. (2004). Timing and Checkpoints in the Regulation of Mitotic
924 Progression. *Developmental Cell, 7*(1), 45-60.
925 Metz, C. W. (1916). Chromosome studies on the Diptera. II. The paired association of chromosomes in
926 the Diptera, and its significance. *Journal of Experimental Zoology, 21*(2), 213-279.
927 Miura, T., & Blakely, W. F. (2011). Optimization of calyculin A-induced premature chromosome
928 condensation assay for chromosome aberration studies. *Cytometry Part A, 79A*(12), 1016-1022.
929 Morais da Silva, S., Moutinho-Santos, T., & Sunkel, C. E. (2013). A tumor suppressor role of the Bub3
930 spindle checkpoint protein after apoptosis inhibition. *J Cell Biol, 201*(3), 385-393.
931 Musacchio, A. (2015). The Molecular Biology of Spindle Assembly Checkpoint Signaling Dynamics.
932 *Current Biology, 25*(20), R1002-R1018.
933 Orr, B., Bousbaa, H., & Sunkel, C. E. (2007). Mad2-independent Spindle Assembly Checkpoint Activation
934 and Controlled Metaphase–Anaphase Transition in Drosophila S2 Cells. *Mol Biol Cell, 18*(3), 850-
935 863.
936 Östergren, G. (1944). Colchicine Mitosis, Chromosome Contraction, Narcosis And Protein Chain Folding.
937 *Hereditas, 30*(3), 429-467.
938 Painter, T. S. (1933). A New Method for the Study of Chromosome Rearrangements and the Plotting of
939 Chromosome Maps. *Science, 78*(2034), 585-586.
940 Painter, T. S. (1934). A New Method for the Study of Chromosome Aberrations and the Plotting of
941 Chromosome Maps in Drosophila Melanogaster. *Genetics, 19*(3), 175-188.
942 Pandey, R., Heidmann, S., & Lehner, C. F. (2005). Epithelial re-organization and dynamics of progression
943 through mitosis in Drosophila separase complex mutants. *Journal of Cell Science, 118*(4), 733-
944 742.
945 Pfau, S. J., & Amon, A. (2012). Chromosomal instability and aneuploidy in cancer: from yeast to man.
946 *EMBO reports, 13*(6), 515-527.
947 Prasad, M., Jang, A. C. C., Starz-Gaiano, M., Melani, M., & Montell, D. J. (2007). A protocol for culturing
948 Drosophila melanogaster stage 9 egg chambers for live imaging. *Nature Protocols, 2*(10), 2467-
949 2473.

950 Reed, B. H., & Orr-Weaver, T. L. (1997). The Drosophila gene morula inhibits mitotic functions in the
951 endo cell cycle and the mitotic cell cycle. *Development, 124*(18), 3543-3553.
952 Rodriguez-Bravo, V., Maciejowski, J., Corona, J., Buch, Håkon K., Collin, P., Kanemaki, Masato T., Shah,
953 Jagesh V., & Jallepalli, Prasad V. (2014). Nuclear Pores Protect Genome Integrity by Assembling a
954 Premitotic and Mad1-Dependent Anaphase Inhibitor. *Cell, 156*(5), 1017-1031.
955 Schmidt, W. M., Uddin, M. H., Dysek, S., Moser-Thier, K., Pirker, C., Höger, H., Ambros, I. M., Ambros, P.
956 F., Berger, W., & Bittner, R. E. (2011). DNA Damage, Somatic Aneuploidy, and Malignant
957 Sarcoma Susceptibility in Muscular Dystrophies. *PLoS Genetics, 7*(4), e1002042.
958 Schneider, C. A., Rasband, W. S., & Eliceiri, K. W. (2012). NIH Image to ImageJ: 25 years of image
959 analysis. *Nature Methods, 9*(7), 671-675.
960 Schoenfelder, K. P., Montague, R. A., Paramore, S. V., Lennox, A. L., Mahowald, A. P., & Fox, D. T. (2014).
961 Indispensable pre-mitotic endocycles promote aneuploidy in the Drosophila rectum.
962 *Development, 141*(18), 3551-3560.
963 Sigrist, S. J., & Lehner, C. F. (1997). Drosophila *fizzy-related* Down-Regulates Mitotic Cyclins and Is
964 required for Cell Proliferation Arrest and Entry into Endocycles. *Cell, 90*(4), 671-681.
965 Singer, J. B., Harbecke, R., Kusch, T., Reuter, R., & Lengyel, J. A. (1996). Drosophila brachyenteron
966 regulates gene activity and morphogenesis in the gut. *Development, 122*(12), 3707-3718.
967 Strukov, Y. G., Sural, T. H., Kuroda, M. I., & Sedat, J. W. (2011). Evidence of Activity-Specific, Radial
968 Organization of Mitotic Chromosomes in *Drosophila*. *PLoS Biology, 9*(1), e1000574.
969 Sumara, I., Vorlaufer, E., Stukenberg, P. T., Kelm, O., Redemann, N., Nigg, E. A., & Peters, J.-M. (2002).
970 The Dissociation of Cohesin from Chromosomes in Prophase Is Regulated by Polo-like Kinase.
971 *Molecular Cell, 9*(3), 515-525.
972 Sumner, A. T. (1998). Induction of diplochromosomes in mammalian cells by inhibitors of topoisomerase
973 II. *Chromosoma, 107*(6-7), 486-490.
974 Takanari, H., Nakakuki, K., & Izutsu, K. (1985). Cytogenetic demonstration of out-of-phase DNA synthesis
975 in endoreduplicated CHO. *Cytogenet Cell Genetics, 39*(2), 93-98.
976 Therman, E., Denniston, C., & Sarto, G. E. (1978). Mitotic chiasmata in human diplochromosomes.
977 *Human Genetics, 45*(2), 131-135.
978 Therman, E., Sarto, G. E., & Buchler, D. A. (1983). The structure and origin of giant nuclei in human
979 cancer cells. *Cancer Genetics and Cytogenetics, 9*(1), 9-18.
980 Venken, K. J. T., He, Y., Hoskins, R. A., & Bellen, H. J. (2006). P[acman]: A BAC Transgenic Platform for
981 Targeted Insertion of Large DNA Fragments in D. melanogaster. *Science, 314*(5806), 1747-1751.
982 Vidwans, S. J., DiGregorio, P. J., Shermoen, A. W., Foat, B., Iwasa, J., Yakubovich, N., & O'Farrell, P. H.
983 (2002). Sister Chromatids Fail to Separate during an Induced Endoreplication Cycle in Drosophila
984 Embryos. *Current Biology, 12*(10), 829-833.
985 White, M. J. D. (1935). The Effects of X-Rays on Mitosis in the Spermatogonial Divisions of Locusta
986 migratoria L. *Proceedings of the Royal Society of London B: Biological Sciences, 119*(812), 61-84.
987 Wirth, K. G., Wutz, G., Kudo, N. R., Desdouets, C., Zetterberg, A., Taghybeeglu, S., Seznec, J., Ducos, G.
988 M., Ricci, R., Firnberg, N., Peters, J. M., & Nasmyth, K. (2006). Separase: a universal trigger for
989 sister chromatid disjunction but not chromosome cycle progression. *J Cell Biol, 172*(6), 847-860.
990 Yuan, K., & O'Farrell, Patrick H. (2015). Cyclin B3 Is a Mitotic Cyclin that Promotes the Metaphase-
991 Anaphase Transition. *Current Biology, 25*(6), 811-816.
992 Zack, T. I., Schumacher, S. E., Carter, S. L., Cherniack, A. D., Saksena, G., Tabak, B., Lawrence, M. S.,
993 Zhang, C.-Z., Wala, J., Mermel, C. H., Sougnez, C., Gabriel, S. B., Hernandez, B., Shen, H., Laird, P.
994 W., Getz, G., Meyerson, M., & Beroukhim, R. (2013). Pan-cancer patterns of somatic copy
995 number alteration. *Nature Genetics, 45*(10), 1134-1140.

996 Zhimulev, I. F., Belyaeva, E. S., Semeshin, V. F., Koryakov, D. E., Demakov, S. A., Demakova, O. V.,
997 Pokholkova, G. V., & Andreyeva, E. N. (2004). Polytene Chromosomes: 70 Years of Genetic
998 Research *International Review of Cytology* (Vol. 241, pp. 203-275): Academic Press.
999 Zielke, N., Korzelius, J., van Straaten, M., Bender, K., Schuhknecht, Gregor F. P., Dutta, D., Xiang, J., &
1000 Edgar, Bruce A. (2014). Fly-FUCCI: A Versatile Tool for Studying Cell Proliferation in Complex
1001 Tissues. *Cell Reports, 7*(2), 588-598.
1002 Zybina, E. V., & Zybina, T. G. (1996). Polytene Chromosomes in Mammalian Cells. In W. J. Kwang (Ed.),
1003 *International Review of Cytology* (Vol. 165, pp. 53-119): Academic Press.
1004 Zybina, T. G., Stein, G. I., & Zybina, E. V. (2011). Endopolyploid and proliferating trophoblast cells express
1005 different patterns of intracellular cytokeratin and glycogen localization in the rat placenta. *Cell*
1006 *Biology International, 35*(7), 649-655.

1007

Figure 1

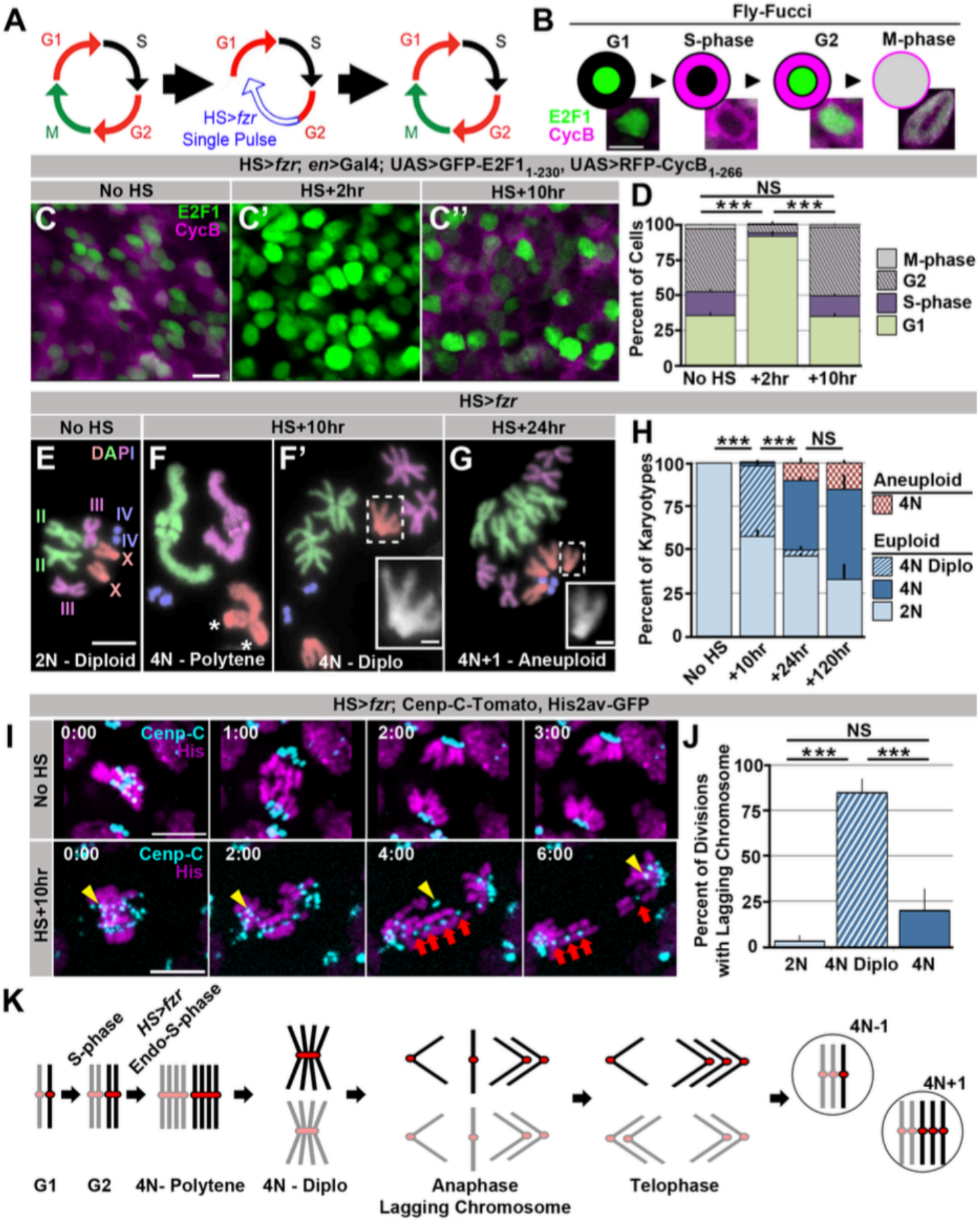

Figure 2

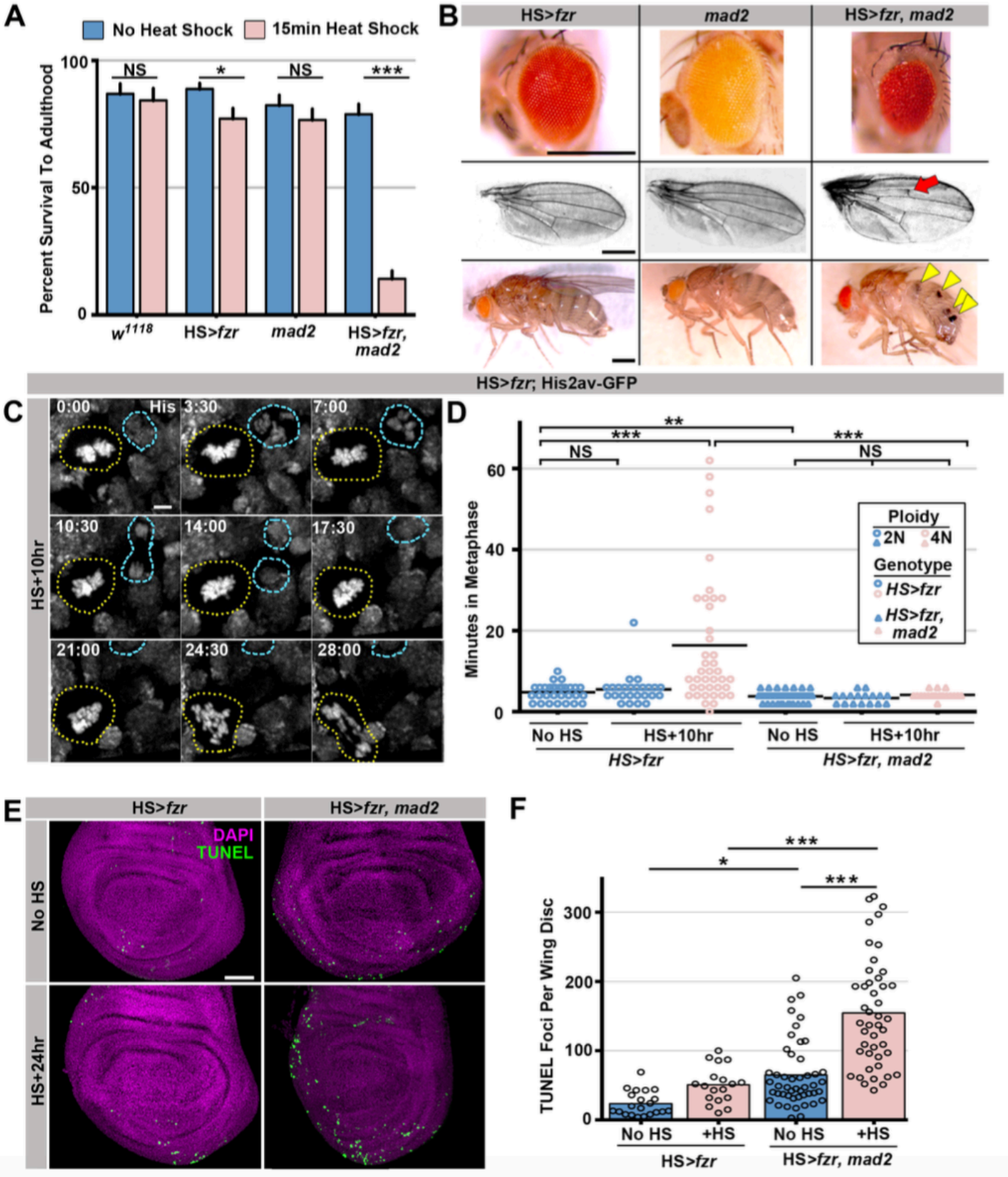

Figure 3

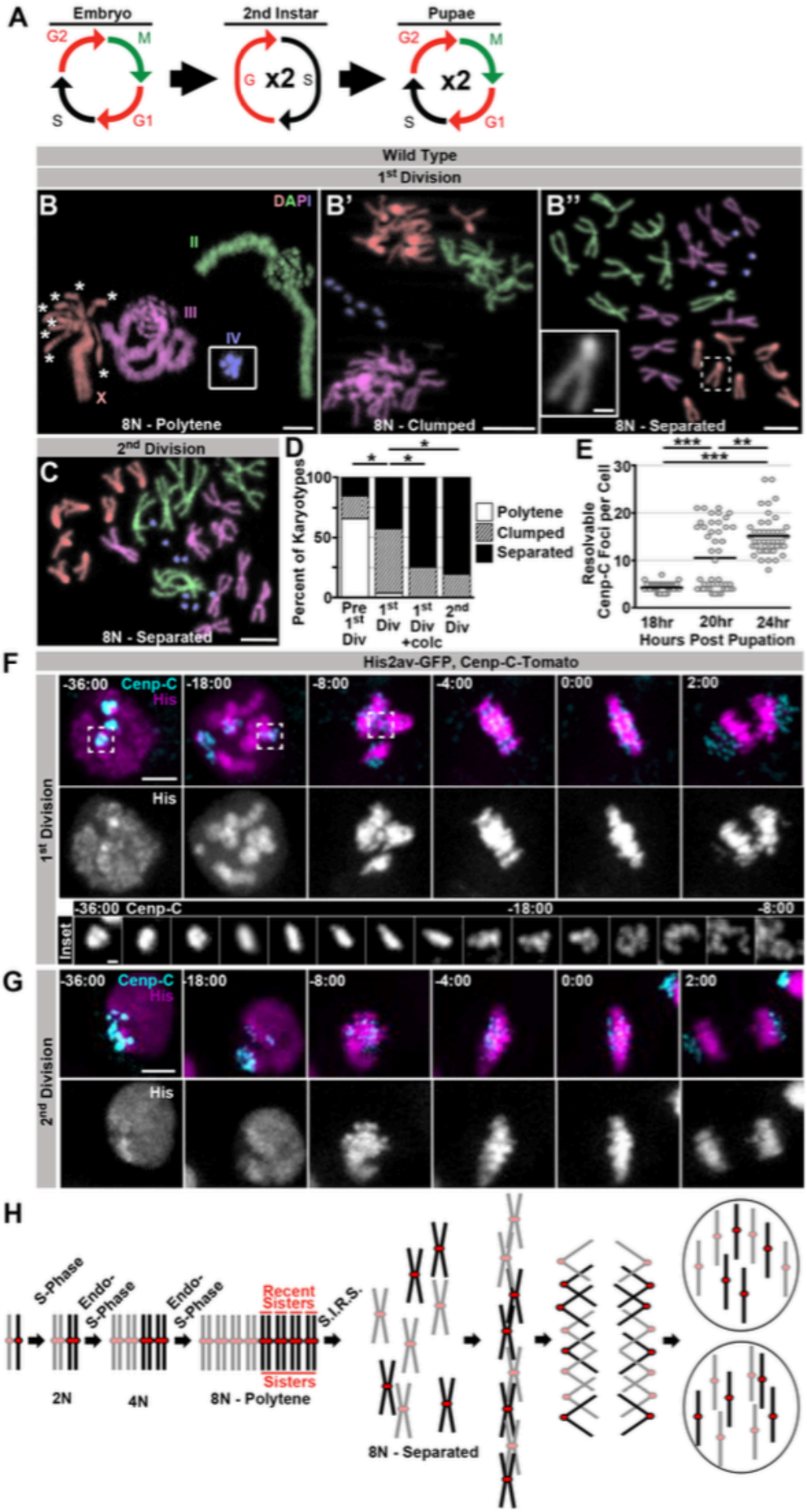

Figure 4

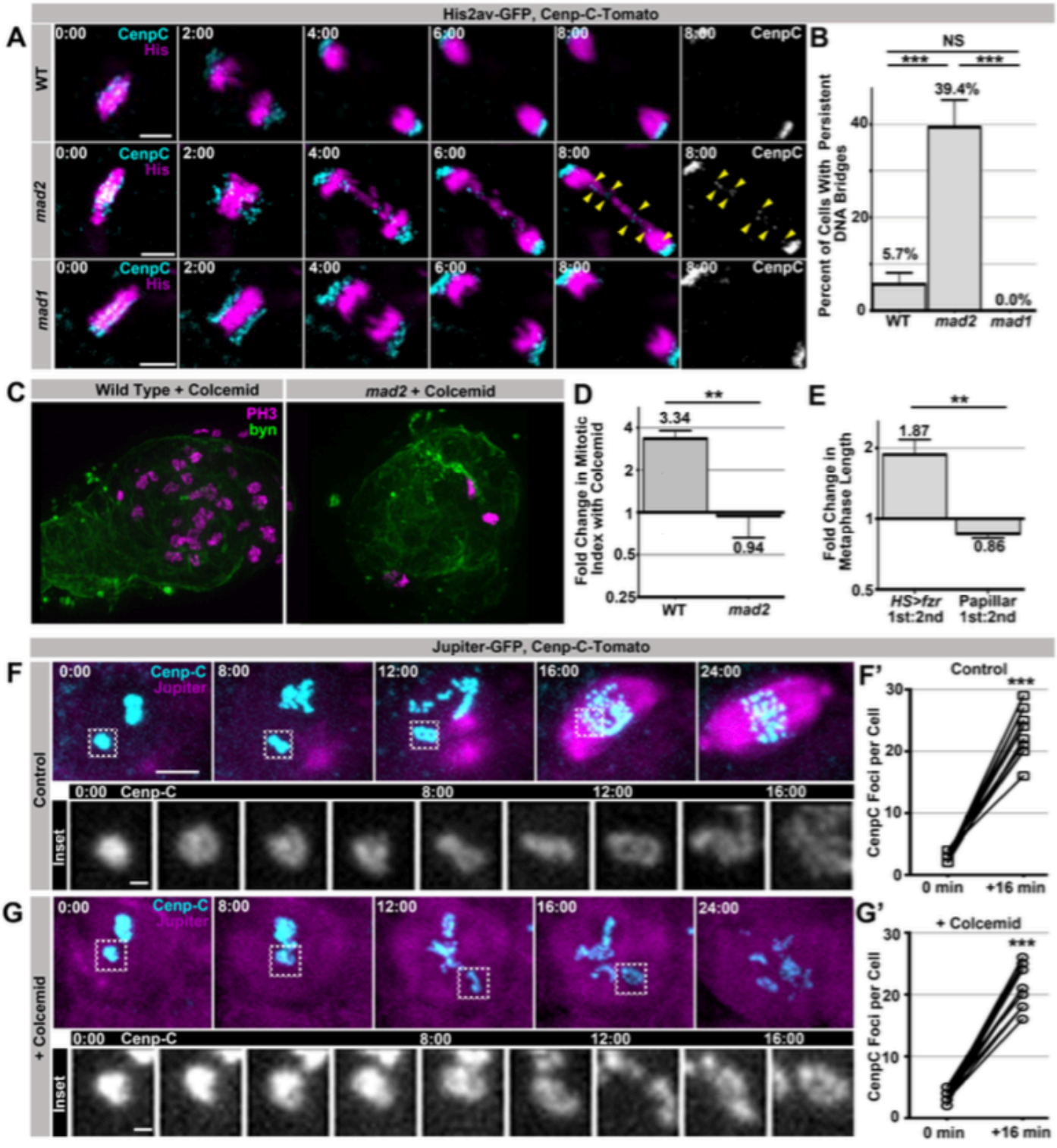

Figure 5

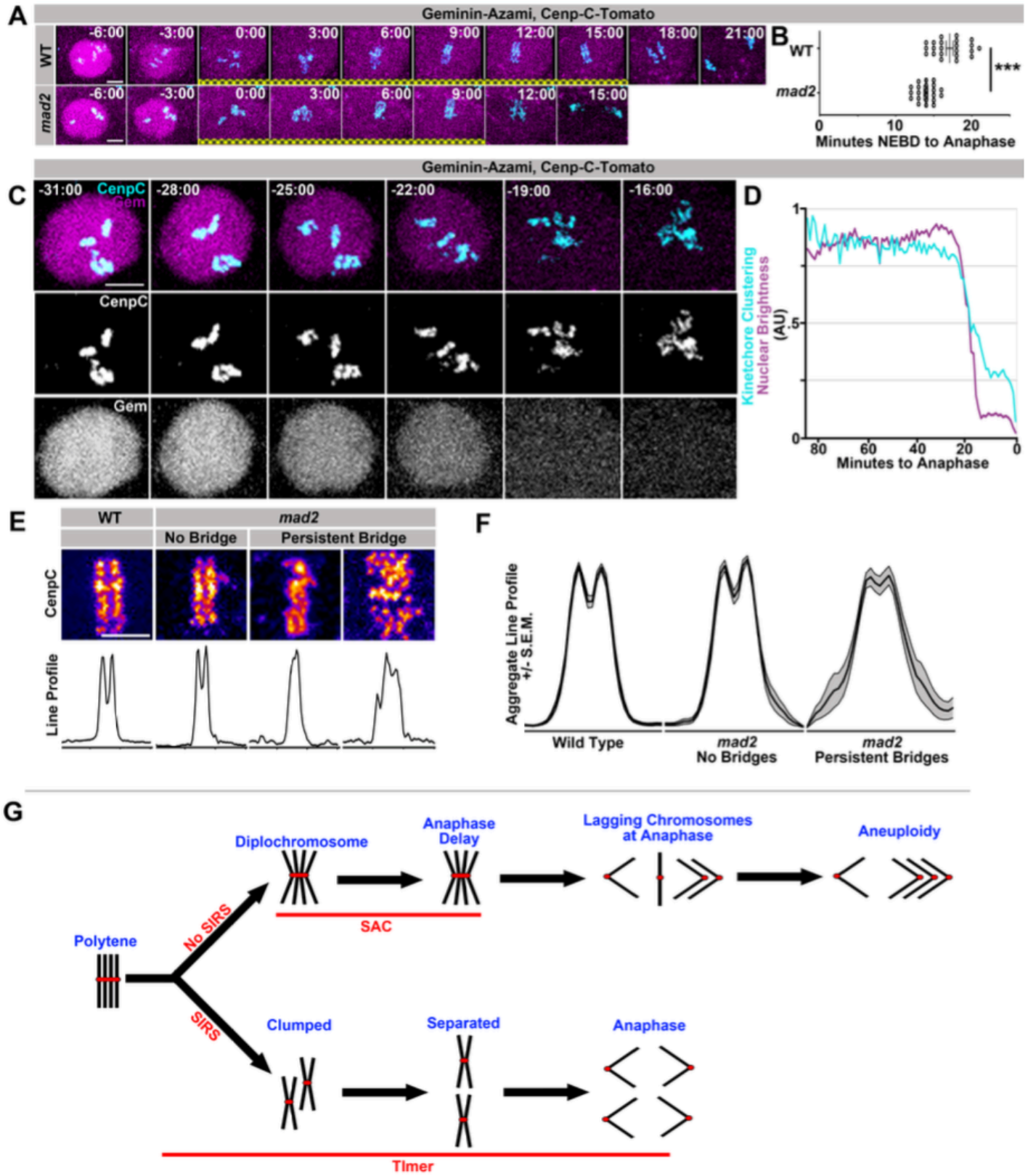

Figure S1

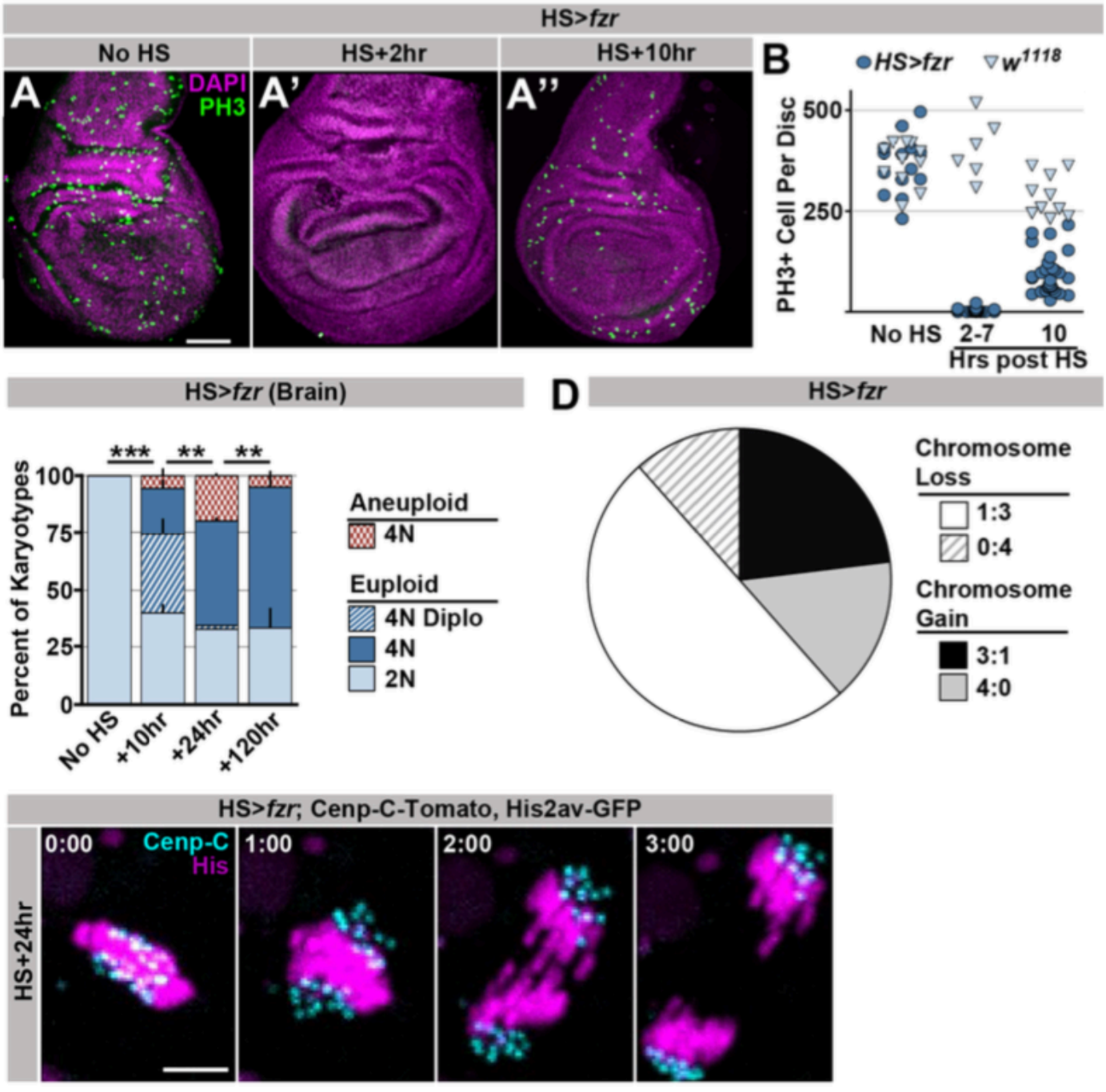

Figure S2

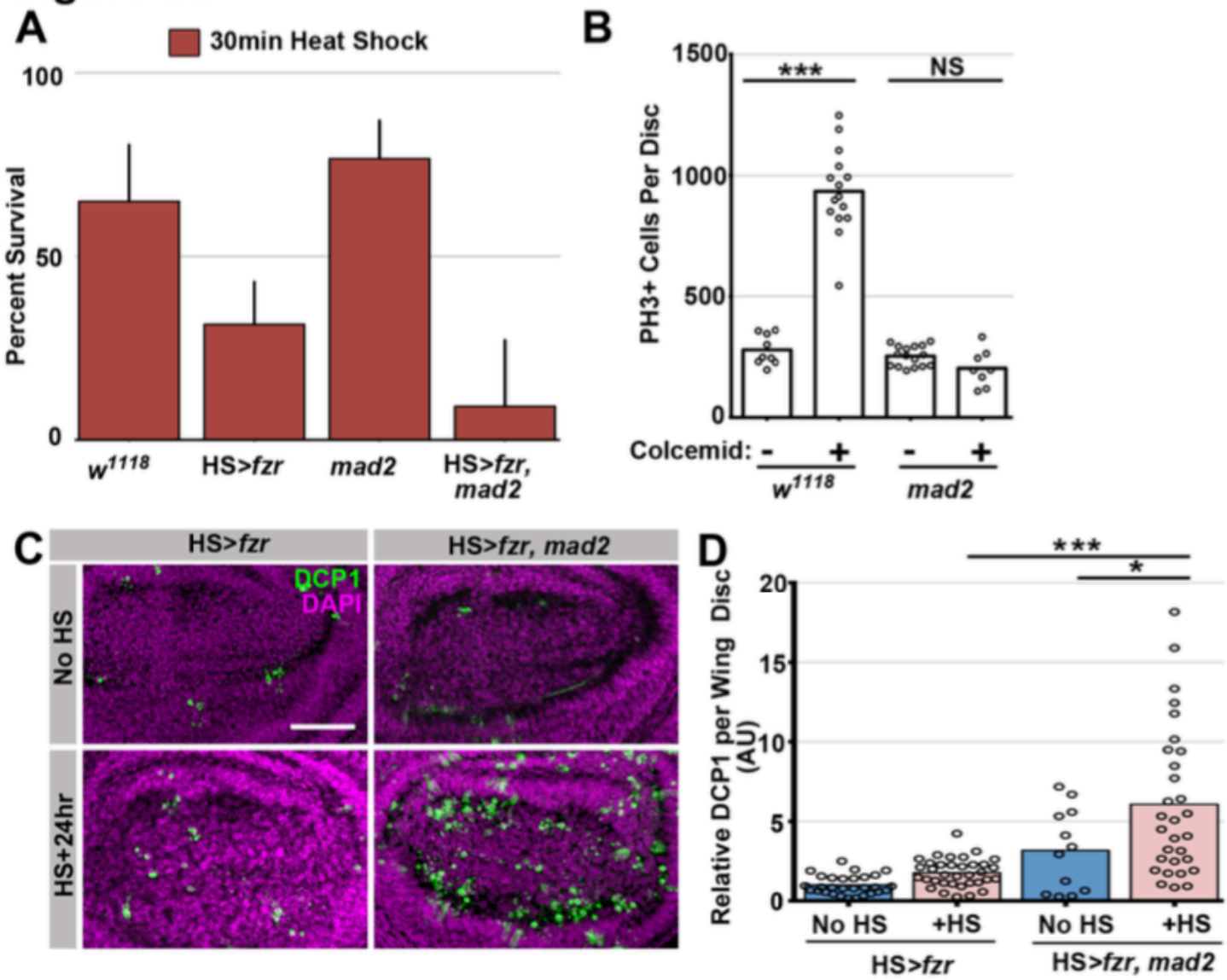

Figure S3